

We are IntechOpen, the world's leading publisher of Open Access books Built by scientists, for scientists

6,900

Open access books available

186,000

International authors and editors

200M

Downloads

Our authors are among the

154

Countries delivered to

TOP 1%

most cited scientists

12.2%

Contributors from top 500 universities



WEB OF SCIENCE™

Selection of our books indexed in the Book Citation Index
in Web of Science™ Core Collection (BKCI)

Interested in publishing with us?
Contact book.department@intechopen.com

Numbers displayed above are based on latest data collected.
For more information visit www.intechopen.com



Traditional and New Types of Passive Flow Control Techniques to Pave the Way for High Maneuverability and Low Structural Weight for UAVs and MAVs

Mustafa Serdar Genç, Kemal Koca,
Hacımurat Demir and Halil Hakan Açikel

Additional information is available at the end of the chapter

<http://dx.doi.org/10.5772/intechopen.90552>

Abstract

Prevailing utilization of airfoils in the design of micro air vehicles and wind turbines causes to gain attention in terms of determination of flow characterization on these flight vehicles operating at low Reynolds numbers. Thus, these vehicles require flow control techniques to reduce flow phenomena such as boundary layer separation or laminar separation bubble (LSB) affecting aerodynamic performance negatively. This chapter presents a detailed review of traditional passive control techniques for flight vehicle applications operating at low Reynolds numbers. In addition to the traditional methods, a new concept of the pre-stall controller by means of *roughness material, flexibility* and *partial flexibility* is highlighted with experimental and numerical results. Results indicate that passive flow control methods can dramatically increase the aerodynamic performance of the aforementioned vehicles by controlling the LSB occurring in the pre-stall region. The control of the LSB with new concept pre-stall control techniques provides lift increment and drag reduction by utilizing significantly less matter consumption and low energy. In particular, new types of these methods presented for the first time by the chapter's authors have enormously influenced the progress of separation and LSB, resulting in postponing of the stall and enhancing the aerodynamic performance of wind turbine applications.

Keywords: energy harvesting recovery, passive flow control techniques, partial flexibility, pre-stall control mechanisms

1. Introduction

Boundary layer transition and separation phenomena have been researchable topics for over 100 years, but there are still many open essential issues and practical challenges containing their controls. It is predicted that the fuel cost of a commercial aircraft could be saved to 8% if the transition phenomenon over its wing could be delayed to 50% [1]. These flow phenomena commonly occur at low Reynolds numbers (Re) at which laminar flow is dominant. A laminar boundary layer can separate from the solid surface when the adverse pressure gradients (APGs) play a preponderant role. Transition phenomenon in the separated region is caused by the separated shear layer, and then the turbulent reattachment starts to occur because of energized vortical structures. The region between separation and reattachment points is called as laminar separation bubble [2, 3] (LSB), which negatively affects the aerodynamic performance. LSBs can form in many aeronautical applications operating in low Re regime of less than 1×10^6 and angle of attack (AoA) of less than stall angle, such as high latitude aircrafts, micro air vehicles (MAVs), multielement airfoil configurations, unmanned aerial vehicles (UAVs), wind turbine, and low-pressure turbine blades.

As stated above, the aerodynamic efficiency can be severely decreased by LSBs by reducing the lift and increasing the drag forces. Besides this, it causes the increment of unsteadiness and noise, especially for wind turbine applications. Regarding a better understanding of LSBs' topology, they can be categorized as 'short' and 'long' bubbles. Aerodynamic researchers recommended a few parameters so that LSBs could be classified whether they are 'short' or 'long' [3–5]. Assessment of effects of either 'short' or 'long' bubbles on the pressure distribution can be the best option and intuitive way. If the pressure field is drastically affected by strong downstream and upstream impacts, it is 'long'. But, if the LSB causes the local and limited impacts on the pressure distribution, it is 'short'. LSBs have an unsteady separated shear layer because of the small disturbances and these disturbances cause the vortical structures to grow rapidly. The separation and reattachment points are affected by these structures and they inherently cause the shape and size of the separated region to change. Therefore, the laminar to turbulent transition and the instability procedures significantly affect the unstable characteristics of LSBs and the mean flow topology [6–8]. Toward this end, a comprehensive understanding of the concerning physical mechanisms of separation and transition procedures is necessary. This may be concluded with beneficial separation prediction tools, which can result in the development of geometrical structures hydrodynamically and aerodynamically. The probability of active and passive flow control techniques, which cause the negative effects of separation and LSBs to suppress (or at least diminish), may also be revealed by means of these understandings.

The objective of this study is to elucidate the traditional passive control techniques for wind turbine applications operating at low Reynolds number regimes. Besides the explanation of traditional low Reynolds number flow control methods such as VGs etc., new concept pre-stall control mechanisms such as roughness material, flexibility and partially flexibility as mentioned in detailed experimental studies will be enormously highlighted.

2. Low Reynolds number aerodynamics

The aerodynamic performances of airfoils in low Reynolds number flows considerably relate to a major range of engineering applications. The low Reynolds number flows are described that the viscous forces within fluid gain dominant characterization compared with inertial forces. Hereby, boundary layer physics such as laminar boundary layer separation, reattachment, and transition phenomena can frequently occur at low Reynolds number flows, affecting the performance of airfoils with the important changes of lift and drag forces.

2.1. Transition modes

2.1.1. Natural transition

Given there was an inflection point in the velocity profile, it was proposed that all boundary layer profiles were unstable according to inviscid stability theory. Prandtl [9] later explained a physical prediction of transition and then Tollmien [10] proved it mathematically that viscous instability waves (often identified as Tollmien-Schlichting (hereinafter TS) waves) could cause a laminar boundary layer to destabilize. But these findings were not accepted by aerodynamic researchers until the study performed by Schubauer and Skramstad [11], since the early experimental investigation for transition prediction had large free-stream turbulence level.

Now, the free-stream turbulence level is accepted as low when it is less than 1% (<1%) [12]. In that flow case, a laminar boundary layer becomes linearly unstable when the critical Reynolds number is increased, showing TS waves that have started to grow.

The sketch of the natural transition process is indicated in **Figure 1**. The flow in the area indicated by number 1 is laminar. In the area denoted by number 2, TS waves start to grow. After that point, the transition to turbulence may not be concluded every time due to the slow growth of TS waves. In aerodynamic literature, the regular transition starts to occur after the nonlinear waves have taken place. It can be said that the transition to turbulence is inevitable

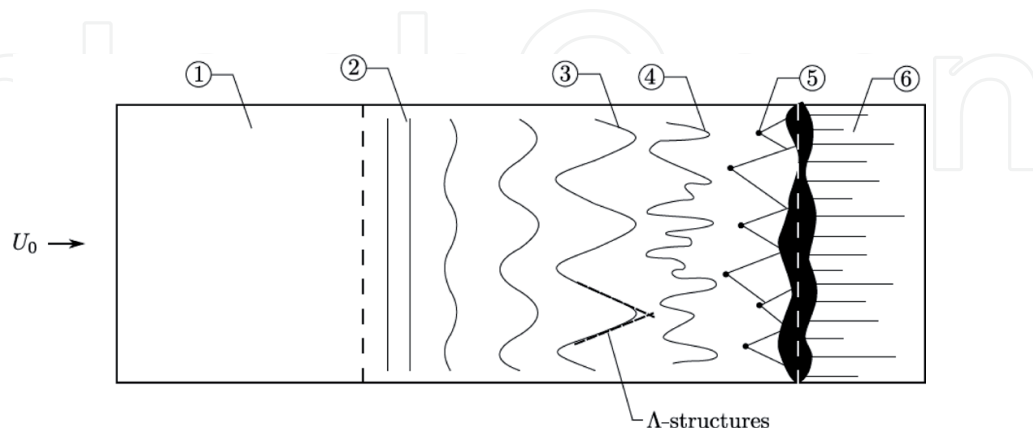


Figure 1. The sketch after Kurelek [13], Bertolotti [14] and Schlichting and Gersten [15] with regard to top view of simplified flat plate boundary layer transition. (1) Laminar flow, (2) TS waves, (3) three-dimensional waves and Λ -structure formation, (4) vortex breakdown, (5) turbulent spots formation, (6) turbulent flow.

after Λ -structures and three-dimensional disturbance defined as nonlinear waves in the area of number 3 and 4. Once those structures form, spots spread in all directions, resulting in the existing turbulent boundary layer as shown in numbers of 5 and 6, respectively.

2.1.2. Bypass transition

Another type of transition is bypass transition. In this transition phenomenon, 2D instability cases of natural transition shown in **Figure 2** are bypassed when the boundary layer on a flat plate under free-stream turbulence intensity is larger than 1%. But, the explanation of bypass transition has still a mystery when free-stream turbulence level is 1%. Therefore, aerodynamic researchers accept as the boundary among natural and bypass transition as free-stream turbulence level is 1%. As mentioned before, spanwise vorticity and 3D breakdown are bypasses in bypass transition and the turbulence spots are directly produced in the boundary layer.

2.1.3. Separated flow transition

Transition to turbulence can exist in the free shear layer when the laminar boundary layer is separated from a solid surface due to sharp, blunt or rounded leading edges. As explaining physically, the boundary layer is able to overcome the effect of adverse pressure gradients at high Reynolds numbers. But, especially at low Reynolds numbers, the laminar boundary layer cannot overcome the adverse pressure gradient due to lack of momentum in the boundary layer and it separates from the surface. This flow separation can cause the transition in the free shear layer. Moreover, after a while, the separated flow may reattach to the surface, resulting in the formation of the laminar separation bubble.

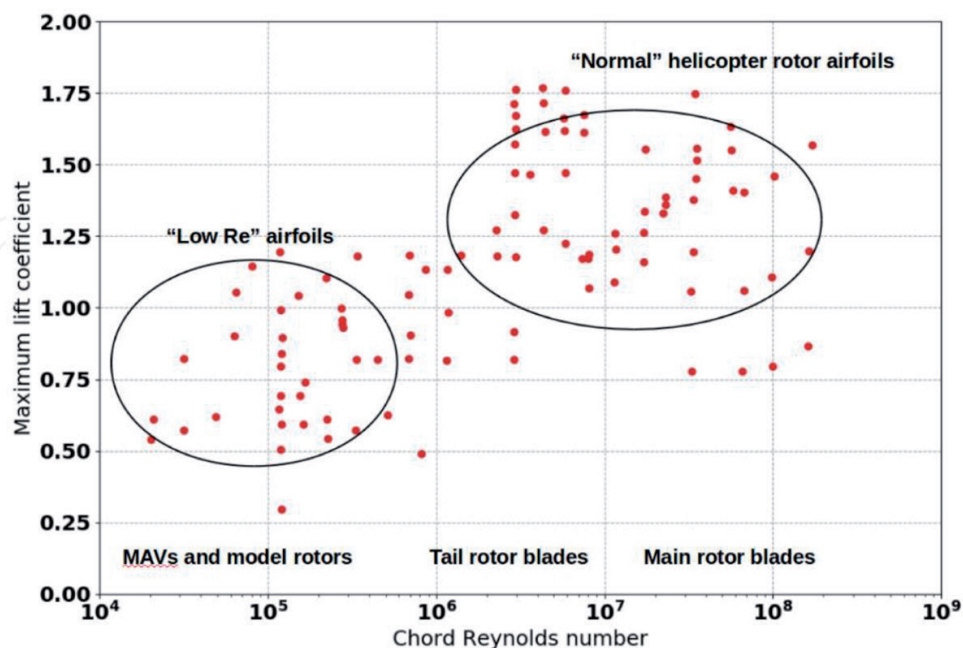


Figure 2. The different rotary wing applications according to variation in chord Reynolds number [18].

2.1.4. Wake-induced transition

This type of transition phenomenon can generally be observed in turbomachinery flows because flows on the blade rows are subjected to periodically impinging wakes coming from the preceding blade rows [16]. In aerodynamic literature, it is suspicious whether enhanced turbulence in the wake or the free-stream level triggers the transition phenomenon. Thus, this type of transition is occasionally distinguished from bypass transition phenomenon and is referred to as wake-induced transition.

2.1.5. Reverse transition

Also known as re-laminarization, the reverse transition is the transition of turbulent to laminar flow. This mode of transition can highly be observed because of high flow acceleration in the regions where favorable pressure gradients play a dominant role. It can be noted that the regions that have favorable pressure gradient generally occur on an airfoil near the leading edge of suction surface and close to the trailing edge of pressure surface. According to the notification carried out by Narasimha and Sreenivasan [17], turbulence dissipation, surface mass transfer, and thermal effects can cause possible reverse transition.

Regarding the different rotary wing applications, the variation of maximum lift coefficient ($C_{L, \max}$) with the chord-based Reynolds number range is shown in **Figure 2** [18]. The fluid flows over airfoils at especially chord-based Reynolds number of 10^4 to 10^5 are more sophisticated due to the dominant character of viscous effects. Despite most regarding studies performed by aerodynamic researchers, low Reynolds number aerodynamics still have researchable potential. This is because of the following: (i) the separated laminar boundary layer because of adverse pressure gradients (APGs) is sensitive; (ii) transition region is too broad, resulting in more unsteady behavior; (iii) short and long separation bubble formations emerge with these APGs and inadequate momentum in flow; and (iv) susceptible role can be played because of surface conditions free-stream turbulence.

Due to these types of flow phenomena mentioned above such as laminar boundary layer separation or LSBs, the detection of flow separation is too important. Flow separation can cause the aerodynamic stall leading to undesired dynamic or static loading statements with a decrease in the lift and an increase in drag for airfoils operating at low Reynolds number ranges. Therefore, flow control methods have been developed to mitigate (to even suppress) their detrimental influences in terms of aerodynamic performances. The flow control mechanism can be divided into two categories as passive and active flow control. The essential difference between active and passive flow control techniques is that some sort of energy input is necessary for active flow control to manipulate the flow, while passive flow control methods manipulate the flow by not requiring any exterior energy resources. These two control methods have advantages and disadvantages compared to each other. One drawback of passive flow control technique can be that it cannot be switched on or off whenever users need. But most aerodynamic researchers have recently preferred the passive flow control methods to provide technologically and economically efficient solutions as long as it does not ensure any undesirable situations except for its design conditions, because they are the

quickest solution to implement processes and less expensive. In spite of the advantages and disadvantages of these two control techniques, they have been tested and researched by aerodynamic researchers with the aim of alleviating the stall effects and enhancing the performance of the overall airfoil.

3. Passive flow control techniques

These types of flow control methods generally improve the condition of flight vehicles by manipulating the flow characteristics in the boundary layer, because the flow manipulation is an efficient way to control mixing in the separated shear layer. So far, aerodynamic researchers have utilized these techniques experimentally or numerically in their studies. A detailed explanation of these passive flow control techniques has been presented as follows:

3.1. Vortex generators

The vortex generators (VGs) as depicted in **Figure 3** [19] are the most effective and simplest passive flow control devices that are widely preferred and utilized on wind turbine blades by aerodynamic researchers in order to prohibit and suppress flow separation caused by APGs. VG examples are not limited to airfoil [20], and they can also utilize the devices such as bluff bodies [21], noise reduction [22], wind turbines [23], swept wings [24], and heat exchangers [25, 26], just to name a few. VGs, which were first investigated by Taylor [27], are generally small plates having rectangular or triangular shapes. They can be mounted on the surface where desired to flow control at an angle of the incoming flow. They are used to decrease (to even suppress) the boundary layer separation, which is caused by APGs and turbulence effects [28]. The slower moving boundary layer is energized by VGs in conjunction with high momentum fluid in the outer part of boundary layer and in the free stream [29], resulting in reducing the drag force [30] and increasing the lift force [31, 32].

Regarding the optimization of VGs, many aerodynamic researchers have investigated the VG's parameters to obtain optimal impacts on fluid flow. As shown in **Figure 4** [33], it can be said that the important parameters are height (h), cropped edge length (b), vane length (L),

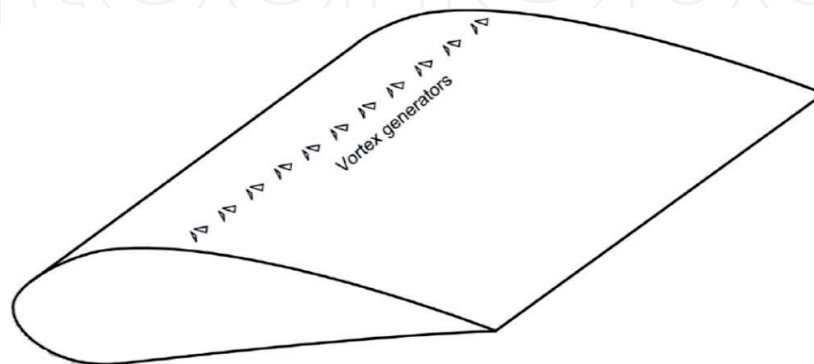


Figure 3. A sketch of vortex generator rows [19].

type, shape, pattern, long (D) and short (d) gaps among the vanes, size, location, and inflow angle (β). In addition to these important parameters, VG configurations termed as counter rotational and corotational also play critical roles in terms of rotational directions of vortices formed by VG pairs [34].

3.2. Leading-edge slats

The leading-edge slats, which were known as a passive flow controller by delaying the flow separation, were initially presented by Handley Page [35] in Great Britain and it was first utilized for an aircraft [36]. As illustrated in **Figure 5** [19, 37], the flow in space between the main body and slat is augmented and accelerated with either large vortices or multiple smaller vortices. Large vortices moving from slat's midspan to its edge can occur at lower Reynolds

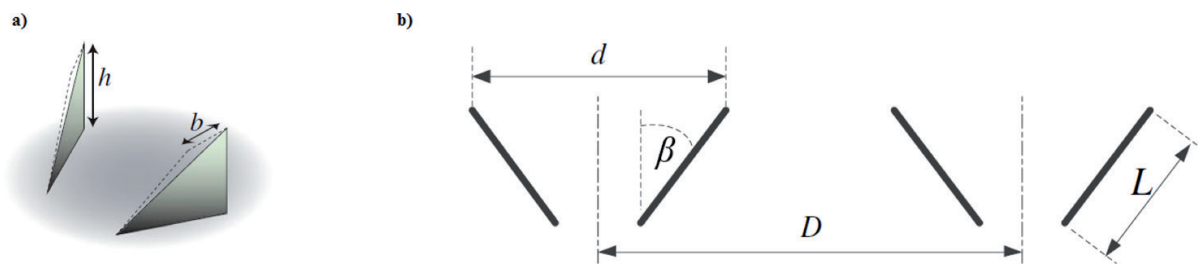


Figure 4. (a) Isometric perspective and (b) planar sketch of the VG row [33].

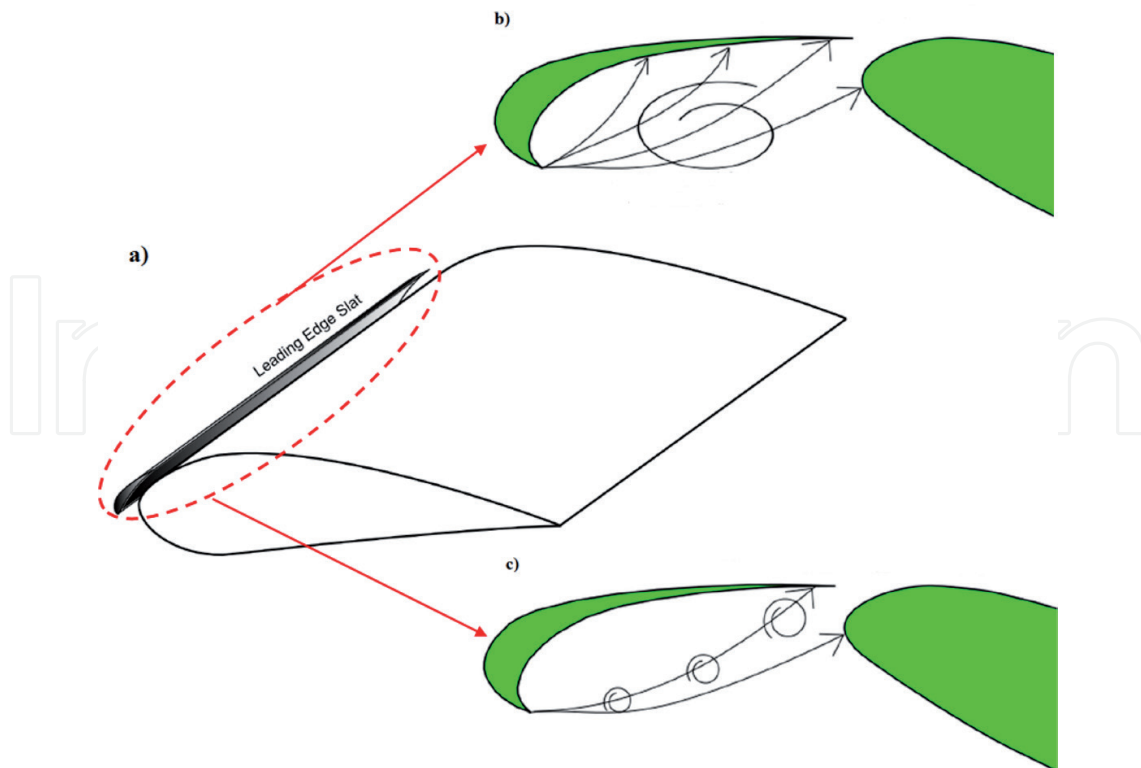


Figure 5. (a) Configuration of leading-edge slat [19] and (b and c) its planar view [37].

number, whereas smaller vortices can be observed at higher Reynolds number. Accelerating flow with leading-edge slats gains kinetic energy and momentum to the boundary layer, resulting in delaying of stall phenomenon [38]. In the literature, there are three types of slats: (i) fixed slat [39], (ii) retractable slat [40], and (iii) Kruger flap [41]. Recently, Genç et al. [42] have investigated NACA2415 airfoil with NACA22 leading-edge slat experimentally and computationally. Their computational results indicated that experimentally stated LSB was correctly estimated. Moreover, delaying of the stall phenomenon was obtained by means of experimental investigation, resulting in providing the maximum lift coefficient of 1.3.

3.3. Flow vanes

The flow vane, which is conceived by Pechlivanoglou [19] and can be utilized as a power regulator and stall controller at wind turbines, is an undiscovered item of the wind turbine blades. As seen in **Figure 6**, the flow vanes have relatively smaller chord length than the main body and this additional aerodynamic profile can be positioned over the suction surface of airfoils. The space among the flow vane and main body is closely equal to the chord length of the flow vane.

3.4. Leading-edge serrations

A passive flow control method entitled as leading-edge serration as shown in **Figure 7** [43, 44] is inspired by the morphology of humpback whales [45]. This bioinspired technique has recently been investigated for different purposes experimentally or numerically. Wang and Zhuang [46] designed a modified wind turbine blades with sinusoidal wave serrations employed on the leading edge to control the boundary layer separation. Their numerical results indicated that the leading-edge serration suppressed the flow separation with the generation of the counter-rotating vortex pairs, especially at high AoA. Cai et al. [47] also numerically investigated a modified airfoil with a single leading-edge protuberance at low Reynolds number. The results showed that the stall angle reduced at the modified airfoil. Furthermore, the pre-stall performance of the modified airfoil decreased, whereas post-stall characteristics were increased. Moreover, an experimental study performed by Wei et al. [48] expressed the hydrodynamic

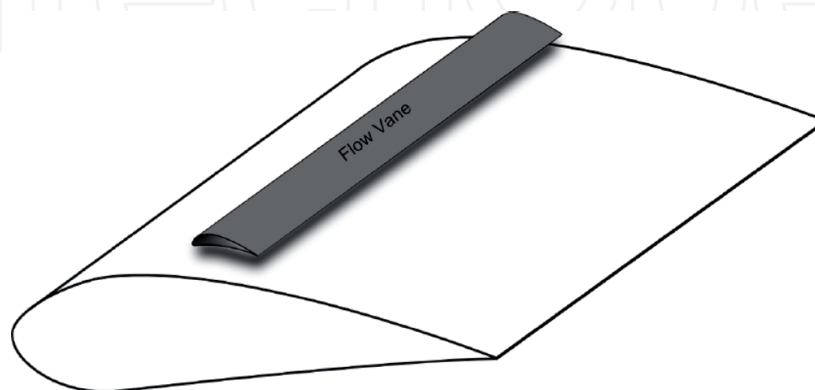


Figure 6. Representation sketch of the flow vane [19].

characteristics of hydrofoils with leading-edge tubercles at Reynolds number of 1.4×10^4 . Their visualization results based on particle tracking revealed that the effects of flow separation were declined with the use of leading-edge tubercles.

3.5. Slotted airfoils

Slots (generally known as a narrow rectangular channel along spanwise of a wind turbine blade) are one of passive flow control methods and flow control is ensured by changing the flow velocity over the airfoil. The principle of a slotted airfoil is that flow velocity increases at the slot exit after interior flow passes within the airfoil. This increment of flow velocity at the slot exit causes the streamlines to disrupt, resulting in creating the flow separation. The flow separation occurred over the airfoil means velocity reduction. This reduction in flow velocity enables the local pressure underneath the airfoil to increase, resulting in producing more lift. **Figure 8** illustrates the slot geometric characteristics performed by Belamadi et al. [49].

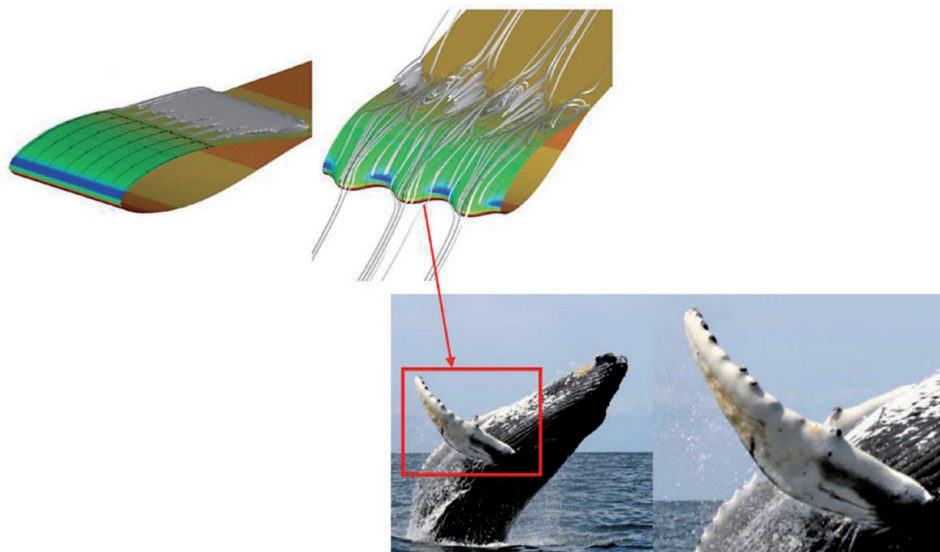


Figure 7. Schematic view of a wind turbine blade with modified models via serrations [43, 44].

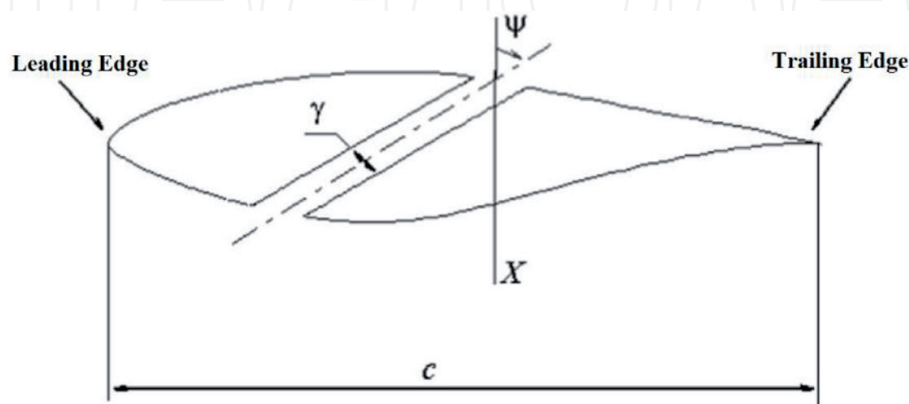


Figure 8. Schematic demonstration of a slotted airfoil [49].

Symbols of c , X , γ , and ψ mean chord of the airfoil, the slot position, the slot width, and angle between slot axis and chord normal, respectively. Numerical results conducted by Belamadi et al. [49] indicated that stall phenomenon on S809 airfoil at an angle of attack of 20° was completely eliminated by creating a nozzle effect over the airfoil, ensuring the extra kinetic energy (inherently extra momentum) to suction surface. Based on experimental and numerical results obtained by Beyhaghi and Amano [50], an increment of the lift coefficient by 30% was ensured without conceding any drag force.

3.6. Leading-edge microcylinder

The leading-edge microcylinders, which are used as passive control technique for boundary layer flow separation, are shown as a whole and enlarged view of mesh domain in **Figure 9** [51]. Regarding the principle of leading-edge microcylinder, velocity over suction surface of the airfoil can be accelerated by them and thus the Kelvin-Helmholtz instability of fluid flow is decreased. As concerning literature studies performed in advance, Luo et al. [52] designed a microcylinder and used in front of the leading edge of NACA0012 airfoil in order to ensure stall delay and decrease the flow separation zone. Based on the numerical calculation carried out by Wang et al. [53], an increment of 27.3% at blade torque was obtained by positioning a microcylinder with a suitable diameter in front of the leading edge.

3.7. Gurney flaps

Gurney flap is a small boundary layer passive control method and it can be easily mounted at the trailing edge of an airfoil. The Gurney flap with 2% of the chord length of the airfoil can affect the aerodynamic performance by increasing the lift coefficient by 0.4. Moreover, the lift-to-drag ratio of the airfoil can be nearly improved by 35% [54]. Flow progress and

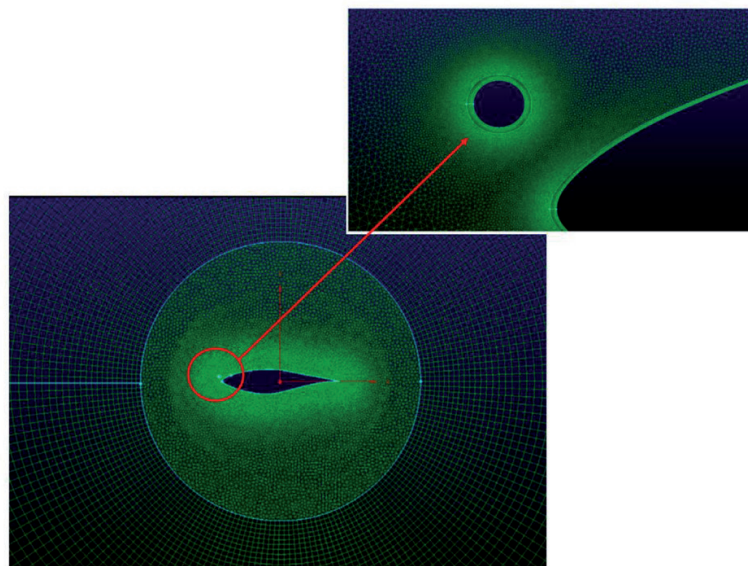


Figure 9. Whole and enlarged view of mesh domain for a leading-edge microcylinder [51].

mechanism of lift increment by the Gurney flap were explained by Liebeck [55]. As depicted in **Figure 10** [55], a pair of counter-rotating vortices composed at downstream of the Gurney flap creates a low-pressure zone within. This low-pressure region makes the flow to increase over the suction surface, resulting in rising to an increase in the suction pressure. On the other hand, the flow velocity is reduced at upstream of Gurney flap by anticlockwise vortices and pressure at the pressure surface is increased. Consequently, the variation of pressure distribution between surfaces leads to an increment of lift force. The unsteady flow characteristics, especially at low Reynolds numbers, may be mitigated and suppressed with the use of Gurney flap. Based on the transient two-dimensional numerical simulations performed by Zhu et al. [56], the adaptive Gurney flap was compared with the fixed Gurney flap and the greater energy harvesting efficiency was obtained when the adaptive Gurney flap was selected for the oscillating wing. Shukla and Kaviti [57] numerically investigated four symmetric NACA airfoils in conjunction with a dimple, Gurney flap and combination of both dimple and Gurney flap at Reynolds number of 3.6×10^5 . Their results indicated that better aerodynamic performance was obtained at NACA0021 airfoil with a combination of both dimple and Gurney flap when the angle of attack was 12° .

3.8. Self-activated deployable flap

Recently, aerodynamic researchers have focused on a technique to palliate the adverse effect of flow and increase the lift coefficient by inspiring the biological flows from birds' wings. Therefore, a self-activated spanwise flap near the trailing edge of the airfoil as a biomimetic device for control of flow separation has been developed as seen in **Figure 11** [58]. Regarding the principle of the self-activated flap, it starts to pop-up because of backflow to cope with critical conditions of flight when flow separation occurs on the suction surface of the wing. Thus, the wing can be prevented from an abrupt increase in the angle of attack because of perching maneuvers or gusts. Rosti et al. [59] investigated physical mechanism of the flow field over NACA0020 airfoil having an elastically mounted flap at Reynolds number of 2×10^4 . It was founded that these flaps could overcome the effect of dynamic stall breakdown causing the abrupt lift loss. In addition, a more positive aerodynamic response such as increasing of lift amount was obtained during the ramp up motion of movable flap. Arivoli and Singh [60] and Schluter [61] also studied self-activated deployable flaps. Their results demonstrated that deployable flaps played crucial roles in terms of aerodynamic performance even though they had a little effect in Reynolds number and heavy stall conditions.

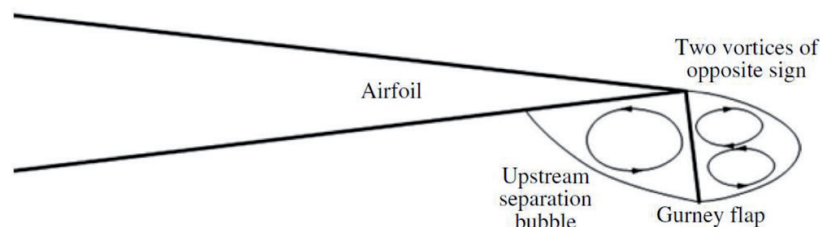


Figure 10. Flow progress at trailing-edge airfoil having a Gurney flap [55].

3.9. Airfoils with cavity

One of the passive control techniques is the application of a cavity mounted on a thick airfoils' suction surface that is taken from original Kasper's wings [62]. The principle of this concept is to create a convenient pressure gradient when two counter-rotating vortices inside the cavity are trapped. Furthermore, these trapped vortices over the suction surface not only ensure an extra low-pressure region but also cause a lower drag to produce. Thus, this method has recently gained interests among aerodynamic researchers. Olsman and Colonius [63] investigated an airfoil with a cavity at Reynolds number of 2×10^4 and different angles of attack ranging from 0° to 15° as seen in **Figure 12**. Their results revealed that stall phenomenon was delayed by means of counter-rotating separated flows, resulted in reduced flow separation region. A detailed numerical study regarding the aeroacoustics of NACA 0018 cavitied airfoil was reported by Lam and Leung [64] at Reynolds number of 2×10^4 and Mach number (Ma) of 0.2.

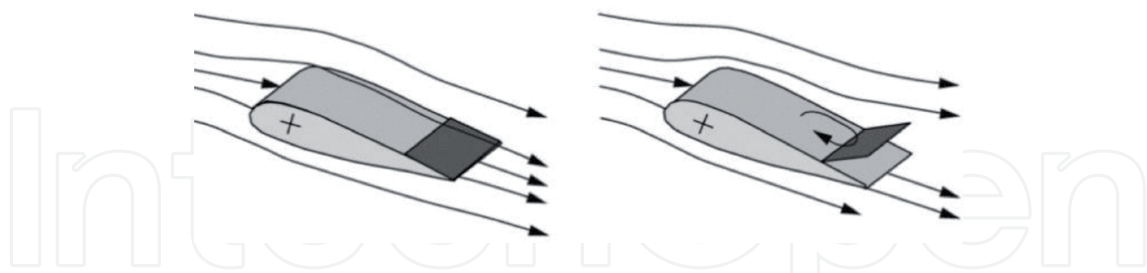
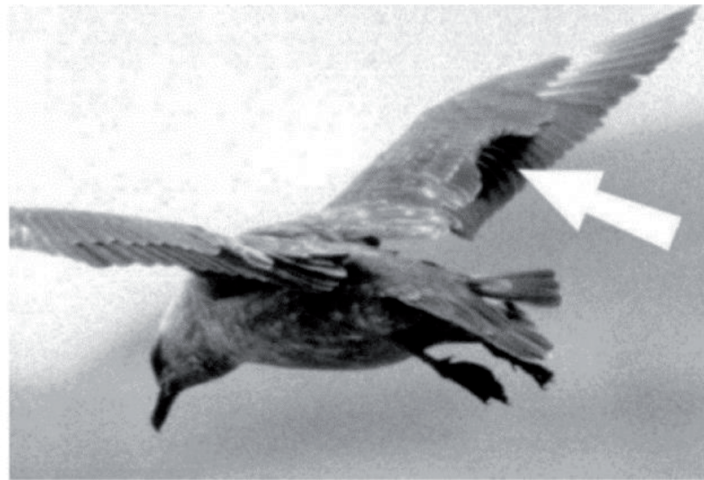


Figure 11. Illustration of a movable flap at a high angle of attack: seagull at landing (top picture) and sketch in principle (bottom picture) [58].



Figure 12. The vorticity contour plot over the airfoil with a cavity [63].

The presence of cavity caused the lift-to-drag ratio to increase. Moreover, cavitied airfoil produced less acoustic power, making it a noiseless airfoil design at low Reynolds number regimes.

3.10. Roughness material

The control technique with the roughness material, which is one of the fundamental objectives of the chapter, can passively control the flow over wind turbine blade operating at low Reynolds number ranges. Regarding the development of vortex structures at the wake of VG applications [65], the flow is re-energized with the vortices produced by miniramps as denoted in **Figure 13**. Furthermore, the flow is inherently gaining momentum by means of that passive flow controller. Therefore, the separated flow because of adverse pressure gradients that occurred generally at leading edge of airfoils may be suppressed with re-energized flows, resulting in the occurrence of more stable flow characteristics without boundary layer separation.

As occurred in VG applications, the flow control method by means of roughness material is performed with similar ways by intervening the flow. Vortex sheds produced by roughness cause the flow in the boundary layer to gain more energy as seen in **Figure 14** [66]. Energized flow hinders the boundary layer flow separation and it ensures the flow to move along the airfoil surface by attaching. The vortex sheds can be used for a few different purposes over the surface of airfoils. For instance, the vortex sheds, which were used for recognition of flow phenomena at the study presented by Koca et al. [67, 68], gave the momentum to flow, resulting in lift recovery and even less vibration or noise for wind turbine blades.

Regarding identifying the role of roughness material on the flow characteristics over roughened NACA 4412 airfoil as indicated in **Figure 15**, investigations based on the force measurement, the smoke-wire, hot-film sensor (glue-on type), and hot-wire experiments have been performed by Genç et al. [8, 69]. The purpose of the experimental study was to determine the LSB and transition phenomena over uncontrolled NACA 4412 airfoil in detail and then was to observe how sandpaper as a roughness material affected the flow topology.

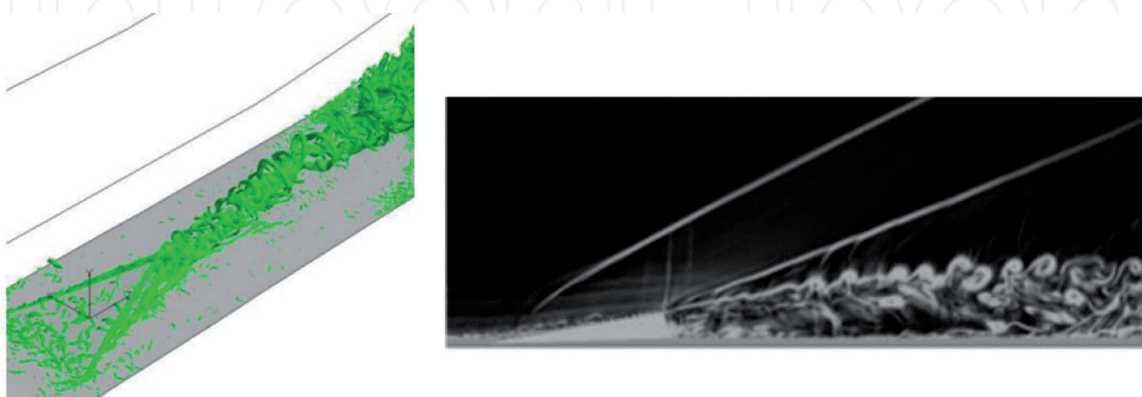


Figure 13. Vortex structures at the wake of VGs [65].

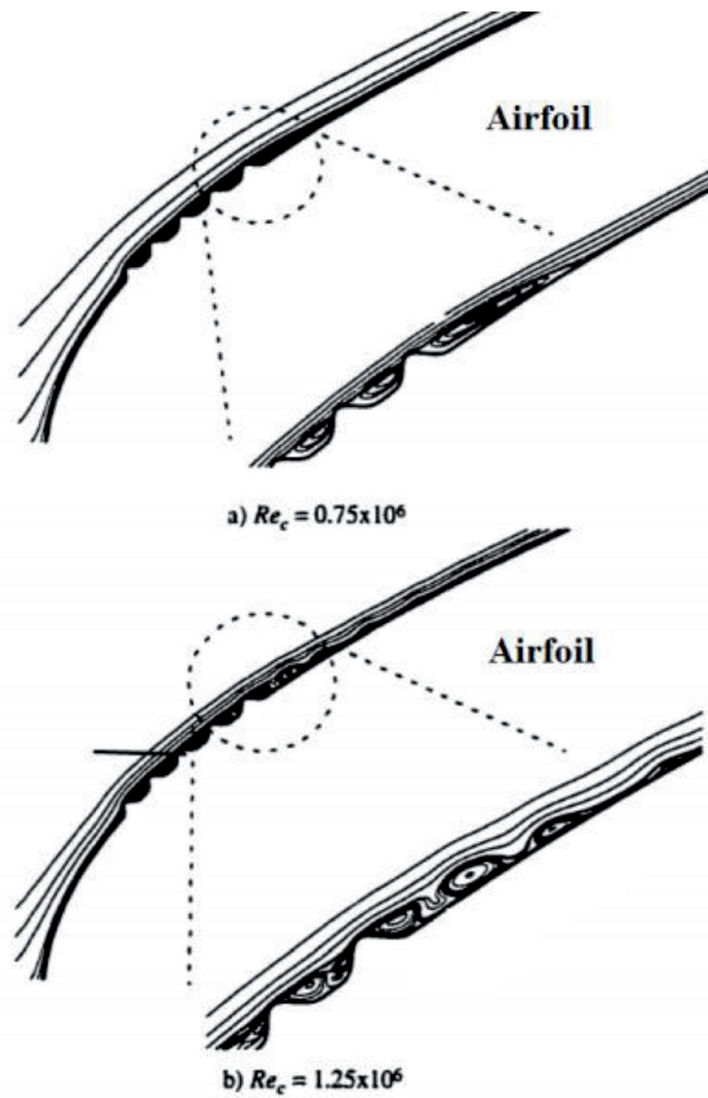


Figure 14. Comparison of 1/4" roughness height and vortex shedding characteristics at different Re_c numbers [66].

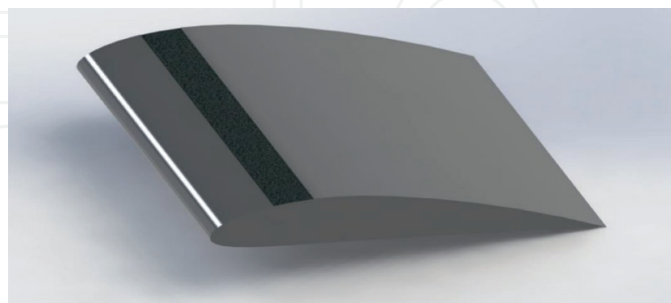


Figure 15. Representation sketch of the roughened airfoil.

The results, which were obtained from smoke-wire experiment and hot-film sensor, showing an integrated graph were denoted in Figure 16 [8]. The streamlines obtained from smoke-wire experiment clearly revealed that LSB occurred between $x/c = 0.3$ and $x/c = 0.7$ for uncontrolled

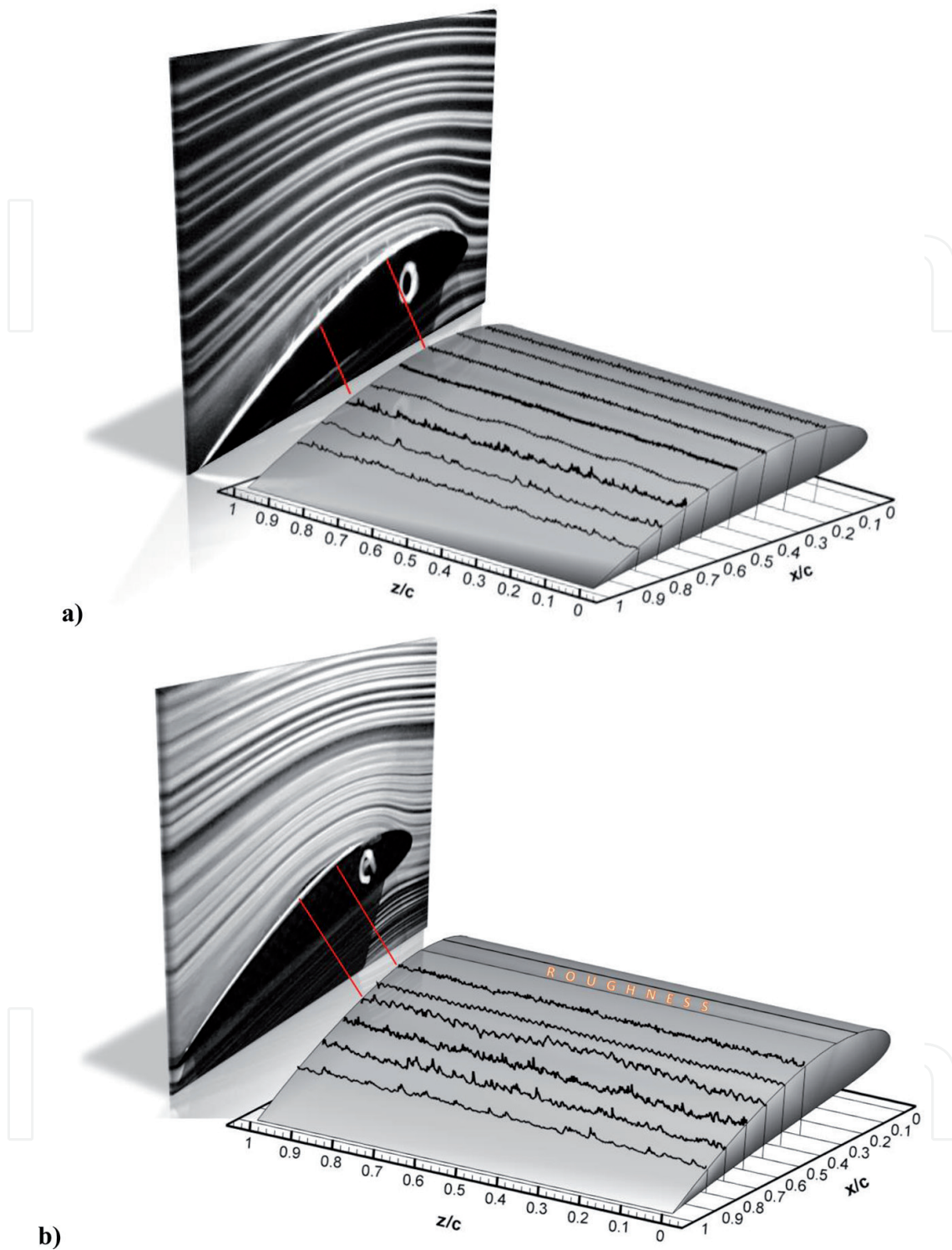


Figure 16. Comparison results of two different experiments at Reynolds number of 5×10^4 and $\alpha = 8^\circ$: (a) $k/c = 0$ (uncontrolled airfoil) and (b) $k/c = 0.003$ [8].

airfoil, while it was seen between $x/c = 0.3$ and $x/c = 0.5$ for the roughened airfoil. It means that using sandpaper causes LSB's size to shrink enormously. As physically speaking, the undulations acquired from voltage values, which were predefined how to obtain in Ref. [8],

started to increase after $x/c = 0.3$, meaning the transition inception and separation point due to adverse pressure gradients in **Figure 16(a)**. However, the amount of undulations at $x/c = 0.5$ was less than that at $x/c = 0.3$, because small eddies having less energy in the aft portion of LSB caused the undulations amount to reduce. After $x/c = 0.5$ point, the obvious increment in undulations indicated that the flow in the boundary layer was fully turbulent because of energized vortices.

Figure 17 [8] shows a combination graph consisting of numerical and experimental results for a roughened airfoil with $k/c = 0.006$ at Reynolds number of 5×10^4 and $\alpha = 8^\circ$. At first glance, APG exhibits a dominant role on flow and it causes the flow to separate from the airfoil surface of $x/c = 0.3$ as depicted in the flow visualization graph. Then, the flow reattaches to solid surface nearly at $x/c = 0.6$ by gaining momentum by means of roughness material. Same flow phenomena like boundary layer separation, reattachment and LSB are shown and proved with streamlines and C_p curves obtained from the numerical study. The peak point among separation (referred to as S) and reattachment (referred to as R) points reveal the LSB in C_p curve. The trend of C_p curve is almost constant after separation point due to the presence of dead air region having as negligible as less flow phenomenon. The position of LSB is between $x/c = 0.3$ and $x/c = 0.6$ as shown in the smoke-wire experiment result. Besides, a mild peak at $x/c = 0.5$ indicates the transition point over the airfoil surface.

In addition to the results mentioned above, two more important results were obtained from aerodynamic force measurement results as seen in **Figure 18**. First, the stall phenomenon because of flow separation was pronouncedly postponed in **Figure 18(a)**. Second, lift coefficient (C_l) in **Figure 18(b)** increased with the use of roughness material, resulting in enhancement of aerodynamic performance of airfoil. Moreover, it was clearly seen that roughness material gave good results, especially in the pre-stall region. Thus, the

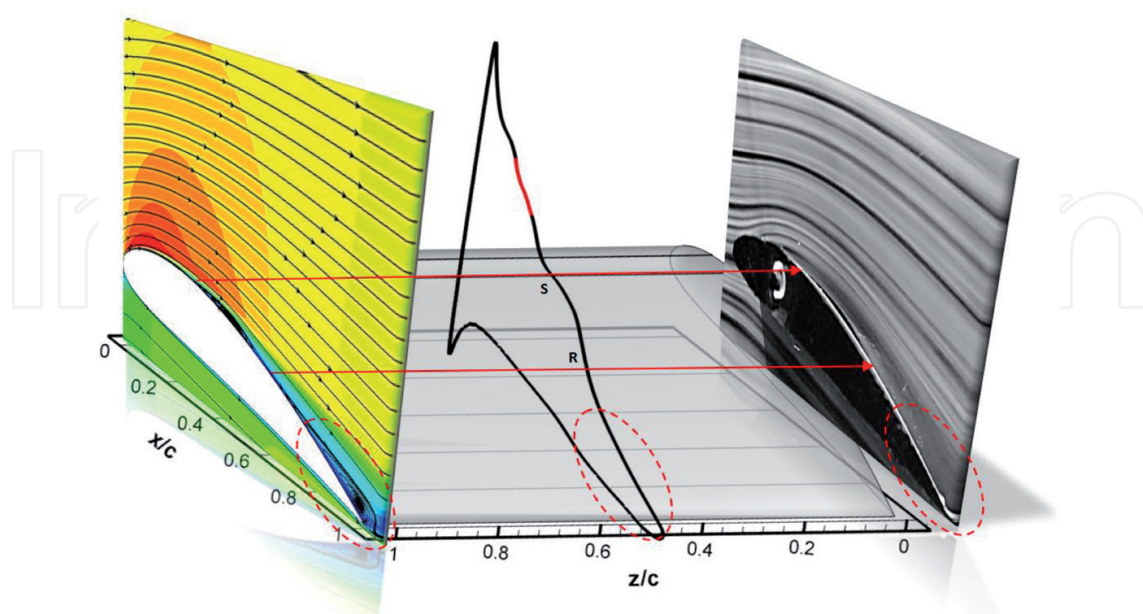


Figure 17. The combined results obtained from the numerical and smoke-wire result for the roughened airfoil with $k/c = 0.006$ at Reynolds number of 5×10^4 and $\alpha = 8^\circ$ [8].

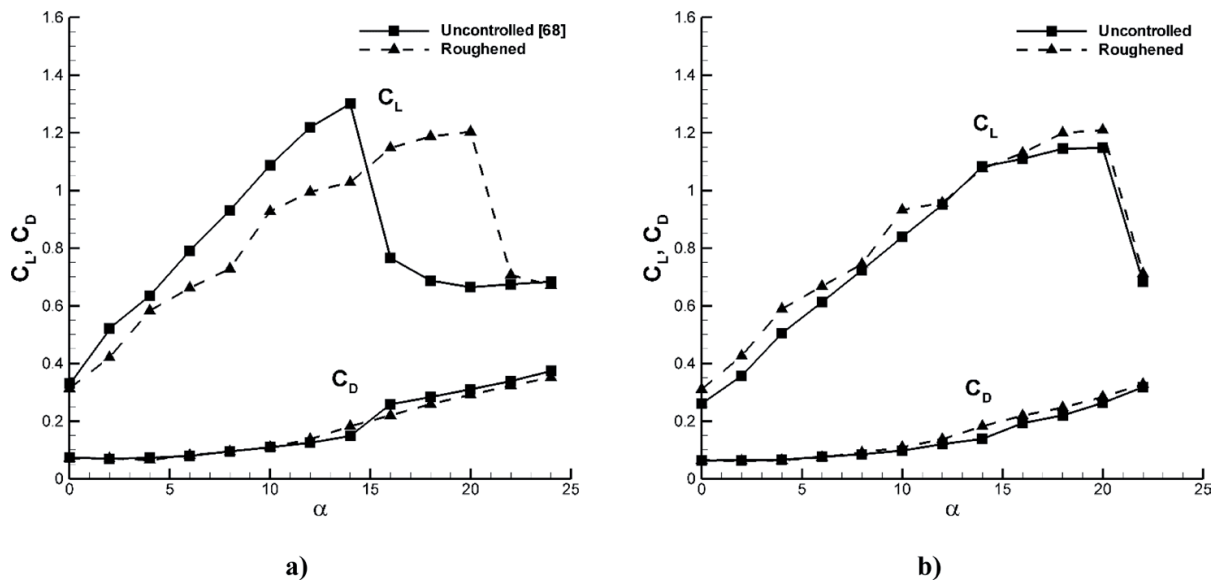


Figure 18. Force measurement results at $k/c = 0.006$: (a) $Re = 7.5 \times 10^4$ and (b) $Re = 1 \times 10^5$ [8].

roughness material was firstly entitled as “the pre-stall flow control mechanism” in aerodynamic literature by authors in Ref. [8].

3.11. Flexible membrane wings

Another essential objective of the chapter in terms of the passive flow control device is doing a detailed survey on flexible membrane wings. The requirement for improving the flight capabilities of MAV and UAV leads to increasing concern in biologically inspired wings. It is well known that the wings of flying animals such as bats resemble a thin membrane-like material with a fixed leading edge and free, scalloped trailing edge that can be easily complied with the flow environment. Moreover, they can regulate the wing planform for a specific flight condition and their flight can be qualified by immensely unsteady and three-dimensional wing motions. A membrane wing is better able to tailor the atmospheric disturbances and makes the vehicle easier to fly [70, 71]. In other respects, the efficacy of the membrane comes from the ability of passive control through the flight as well as decreasing the weight of the wing [70]. Smith [72] paraphrased the emphasis on flexibility and wing stiffness in modeling the flapping motion and generation of the resultant force. A summary presentation study of the aerodynamics of micro air vehicles operating at low Reynolds numbers was carried out by Mueller and DeLaurier [73]. In order to come up with the negative effects of LSB for improving aerodynamic performance, researchers utilized flexible membrane wings for numerous practices such as hang glider, microlight, and UAVs and MAVs. An experimental investigation about time-dependent LSB formation on $AR = 3$ wing was conducted, and it was seen that in the membrane wings at low Re numbers the LSB was more prevalent. Leading-edge separations were influenced via both Reynolds number and leading-edge vortices occurring because of the separation bubbles led to time-dependent alterations on the vibration of the wing [74, 75]. At low AR , tip vortices delayed stall, exclusively at low Re numbers owing to affecting flow on the wing and separation bubble [76] and analysis of the

instant deformation found out spanwise and chordwise, which were due to the shedding of leading-edge vortices' farther tip vortices [77].

Rojratsirikul et al. [78, 79] searched flow and deformation characteristics of membrane wings with low aspect ratio via velocity and deformation measurement. They found membrane oscillations in second chordwise mode at higher incidences. The dynamic of membrane wing can be altered with excess length [80, 81] and support [82] of the wing. Genç [80] studied on a membrane wing with excess length. The results depicted that camber of membrane wing induced the separated flow; therefore, small separated regions were seen. Besides, Greenhalgh et al. [81] observed that increasing excess length caused to reduce separation incidence, and hysteresis interval concluded a restricted working area for the highest excess lengths. Arbós-Torrent et al. [82] considered the effects of the geometry of front and aft of the wing on the aeromechanics of membrane wings. It was stated that average camber-like membrane fluctuations altered with respect to the geometry and size of both front and aft supports. Besides, the front and aft support having rectangular cross-section everlastingly provided further lift and deformations of mean camber compared with circular cross-sectional support. Galvao et al. [83] studied experimentally on the compliant membrane wings modeled based on mammalian flight mechanics. They showed that three-dimensional (3D) flow and tip vortices were ascendant. Furthermore, the deformation of compliant wings increased with both incidence and deformation increasing. Bleischwitz et al. [84] surveyed membrane wings aeromechanics in ground effect. Digital image correlation (DIC) and proper orthogonal decomposition (POD) were used for obtaining membrane vibrations. It was seen that fluctuation modes were adequate to hold 90% of all deformation energy closes to stall. Moreover, structural modes of spanwise were ensured in virtue of POD in lift increment areas. On the other hand, Hu et al. [85] executed a study on the flapping flexible membrane wings. It was seen that oscillation provided significant aerodynamic benefits in unsteady state regime. In other respects, it was concluded that generally the rigid wing had better lift capacity for flapping wings. The flexibility of the wing affected its aerodynamics positively [86] and membrane wings had an increase in maximum C_L during oscillating. Furthermore, an increase in reduced frequency led to an increase in maximum C_L . Membrane wings have a higher slope of lift and postponed stall [87]. Additionally, the membrane kinematics was closely relevant to membrane tension and free-stream velocity [88].

As previously mentioned, numerous studies have been performed for a better understanding of flexible wings and examined their effects in terms of aerodynamic performance. Herein, it is important to give sight for the conducted researches about flexible membrane wing, which are tabulated in **Table 1**. A common result could be said from all these studies that membrane wings had favorable characteristics such as a higher lift-to-drag ratio and a higher maximum lift coefficient when compared to an equivalent rigid wing from the aerodynamics point of view.

Unlike these studies, Demir [98] investigated the deformation that occurred on the flexible membrane wing surface and how it affected the LSB. Moreover, he examined how LSB affected the vibrations that occurred on the membrane surface, the distribution of the flow characteristics, as well as the fluid-structure interactions between the membrane and flow both

Author(s)	Type of wing	Type of study	Working range of Re number
Timpe et al. [71]	Rigid flat plate and membrane wings (AR = 4.3)	Experimental	5×10^4
Rojratsirikul et al. [79, 89, 90]	Rigid and 2D flexible membrane wing		5.31×10^4 , 7.97×10^4 , 10.6×10^4
Rojratsirikul et al. [78]	AR = 2 flexible membrane wing and delta wing		2.4×10^4 – 5.9×10^4
Hu et al. [85]	Cybird-P1® remote control ornithopter model		1×10^4 , 2×10^4 , 8×10^4
Tamai et al. [91]	Flexible membrane wings with different numbers of ribs (FM01, FM02, FM03, FM10)		7.5×10^4
Arbós-Torrent et al. [82]	Membrane airfoils with different geometries of LE and TE support		9×10^4
Bleischwitz et al. [84]	Rigid wing and AR = 2 membrane wing		5.6×10^4
Wrist et al. [92]	Membrane wing with NACA 2504, 4504, 6504, 4404, 4504, 4604, and 4506 frames		5.0×10^4
Attar et al. [93]	Membrane wing		1.37×10^4 , 2.26×10^4 , 3.63×10^4
Galvao et al. [83]	Membrane wing (AR = 0.92)		7×10^4 – 2×10^5
Viieru et al. [94]	Fruit fly (<i>Drosophila</i>)	Numerical	10^4 – 10^5
Hefeng et al. [95]	NACA0012 segmented flexible airfoil		1.35×10^5
Lian and Shyy [96]	Flexible wing (SD7003)		6×10^4
Gordnier and Attar [97]	AR = 2 flexible membrane wing	Both	2.43×10^4
Song et al. [88]	Rectangular membrane wing (AR = 0.9, 1.4, 1.8)	Both	7×10^4 – 2×10^5

Table 1. Summary of pioneering studies on flexible membrane wing.

experimentally and numerically. An experimental study was conducted by Demir and Genç [74] in order to examine time-dependent circumstance of flow on flexible membrane wing and they noticed that the size of LSB altered with time because of the indecisive flow features of the wing. The indecisive behavior upon the flexible membrane wing brought about various deformation modes to constitute at various angles of attack. The results of time-dependent flow visualizations for angles of attack of $\alpha = 12^\circ$ and $\alpha = 10^\circ$ for different time intervals are given in **Figure 19** [75] and **Figure 20** [75]. Time-dependent attitudes of LSB was obviously seen as analogizing obtained results at miscellaneous times between $t = 0.08$ s and $t = 0.20$ s. The bubble size enlarged at $t = 0.16$ s and then was smaller at $t = 0.20$ s for $Re = 2.5 \times 10^4$ at $\alpha = 12^\circ$, as seen in **Figure 19**. Additionally, as it is seen in **Figure 20**, the size of LSB enlarged until $t = 0.12$ s and then lessened at $t = 0.16$ s at $\alpha = 12^\circ$ and $Re = 5 \times 10^4$. For this purpose, it can be deduced that bubble size varied with time because of the indecisive flow characteristics of flexible membrane wing.

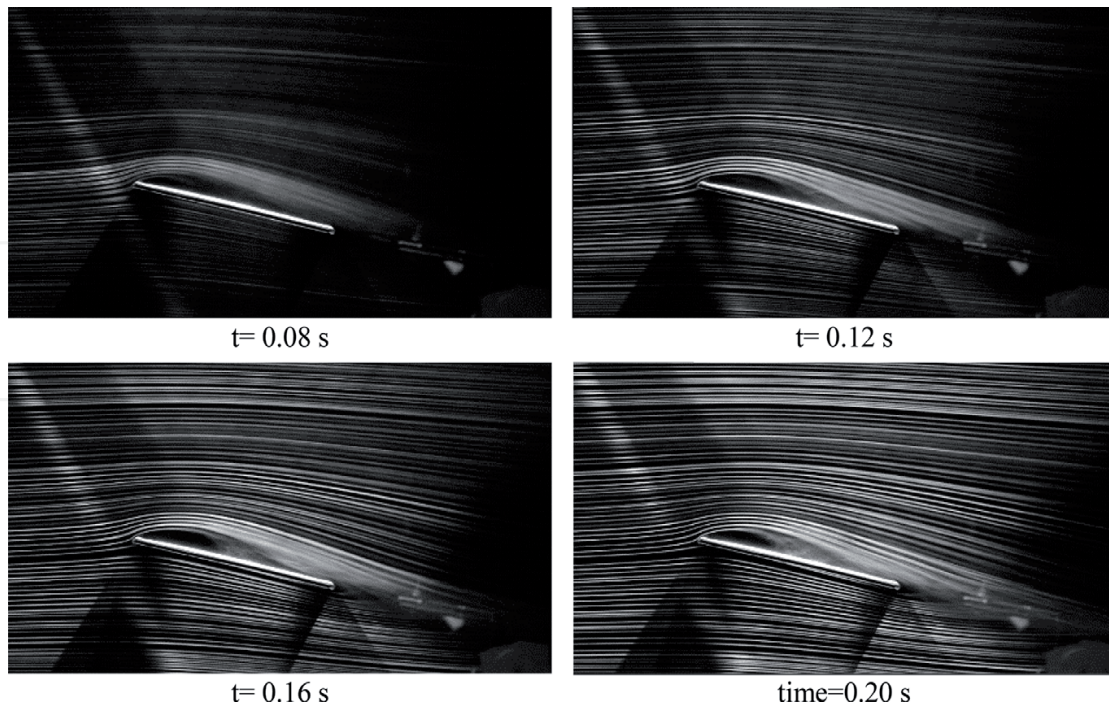


Figure 19. Smoke wire flow visualization result of AR = 3 flexible membrane wing at $y/s = 0.4$ for $\alpha = 12^\circ$ and $Re = 2.5 \times 10^4$ [75].

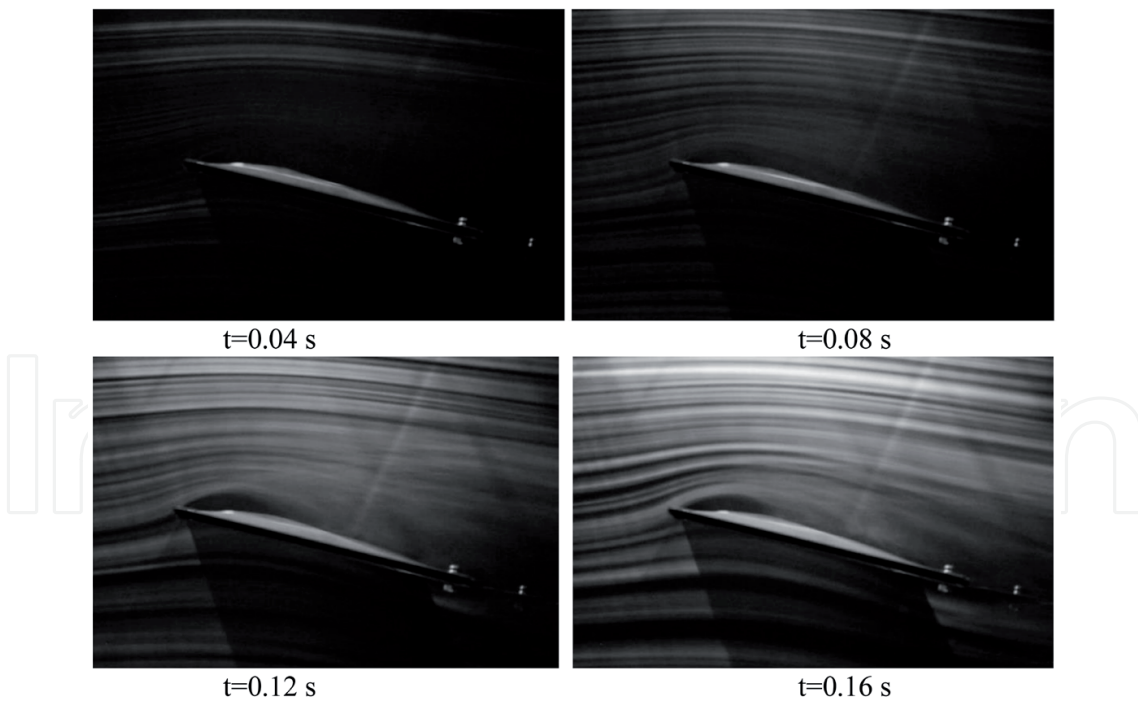


Figure 20. Smoke wire flow visualization result of AR = 3 flexible membrane wing at $y/s = 0.4$ for $\alpha = 10^\circ$ and $Re = 5 \times 10^4$ [75].

As seen in **Figure 21**, vibrational modes in the middle section of the wing reduced and joined up at the tip region at $\alpha = 10^\circ$ by the virtue of occurring separation bubble and these vibrational modes became a chordwise mode of two at $\alpha = 12^\circ$ as seen in **Figure 22**. The holes

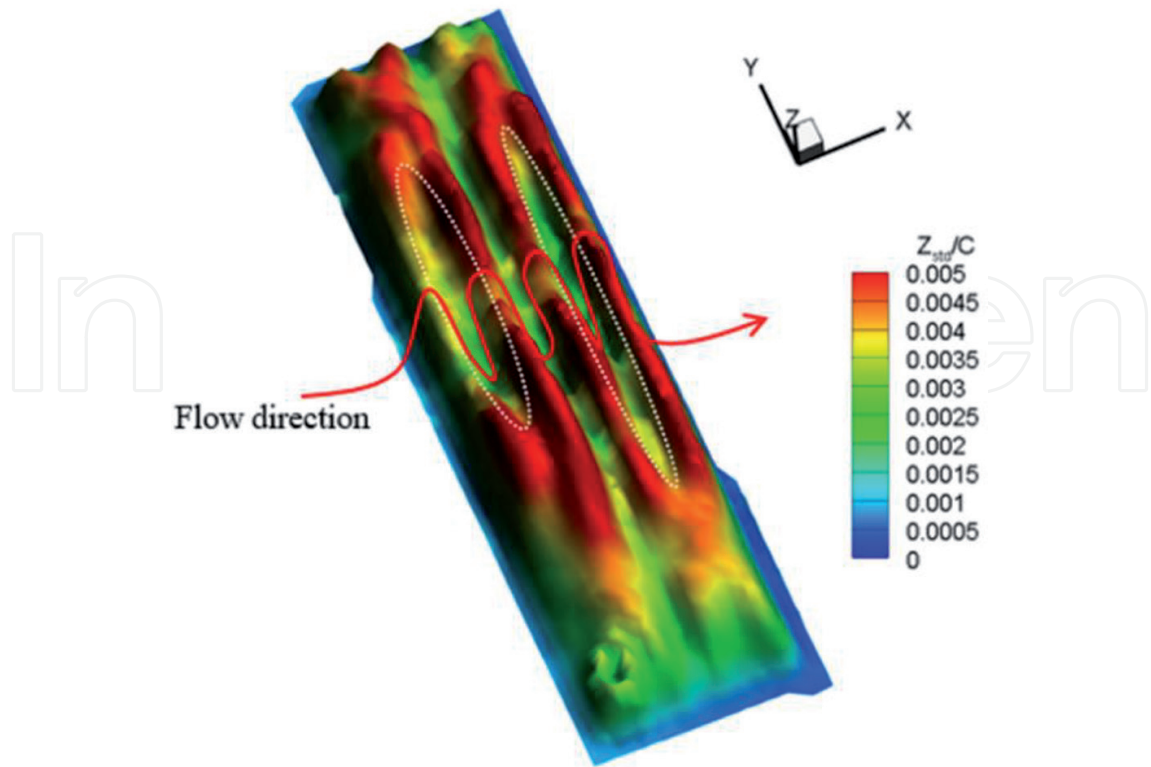


Figure 21. Three-dimensional view of standard deviation of mean deformation of AR = 3 flexible membrane wing at $\alpha = 10^\circ$ for $Re = 5 \times 10^4$.

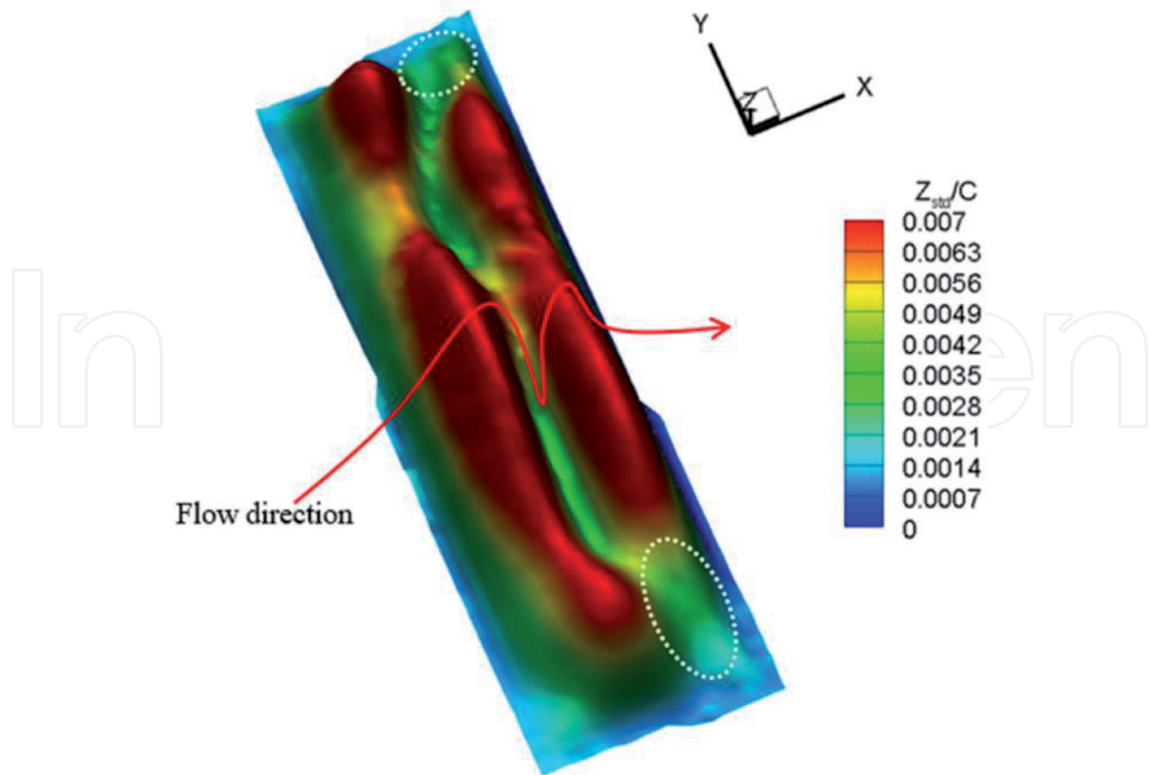


Figure 22. Three-dimensional view of standard deviation of mean deformation of AR = 3 flexible membrane wing at $\alpha = 12^\circ$ for $Re = 5 \times 10^4$.

formed by the separation bubble in the middle of the wing were illustrated with white dashed lines and the regions with red color showed the peaks.

3.12. Partially flexible airfoil

The last major control device, which is the objective of the chapter, among passive flow controllers is the flexible membrane used on the surface of the airfoil. This type of airfoil is called as a segmented or partially flexible airfoil. Since it is a new concept of flow control method, a detailed investigation of a partially flexible membrane is rarely studied in the aerodynamic literature. A pioneered computational fluid dynamics (CFD) analysis was performed using

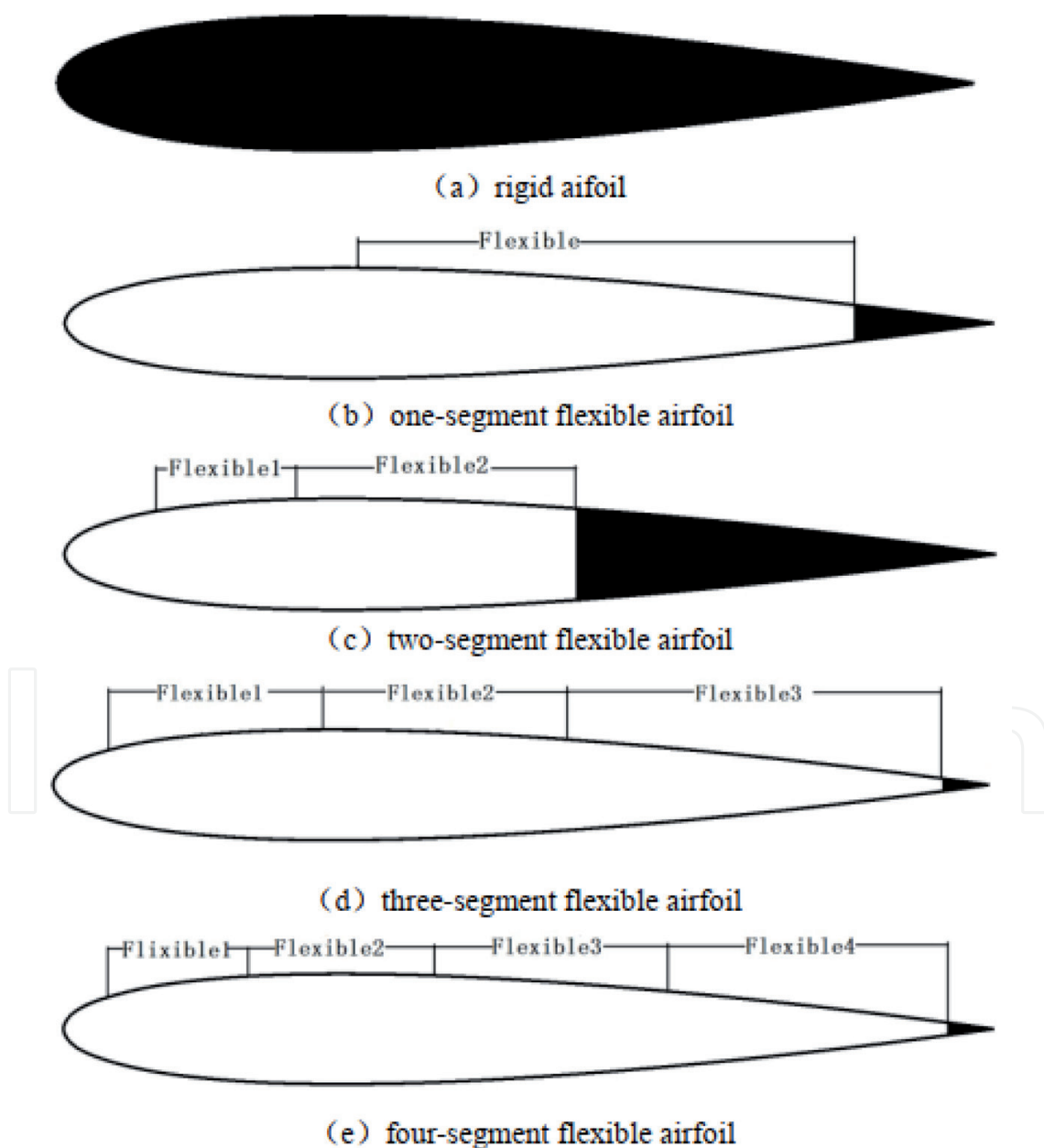


Figure 23. Different types of segmented airfoils [95].

flexible membrane material on the airfoil surface by using ANSYS software [95]. The fluid-structure interaction (FSI) method was used for numerical modeling to investigate interactions between fluid and membrane. The segmented airfoil is seen in **Figure 23** [95]. The flexible

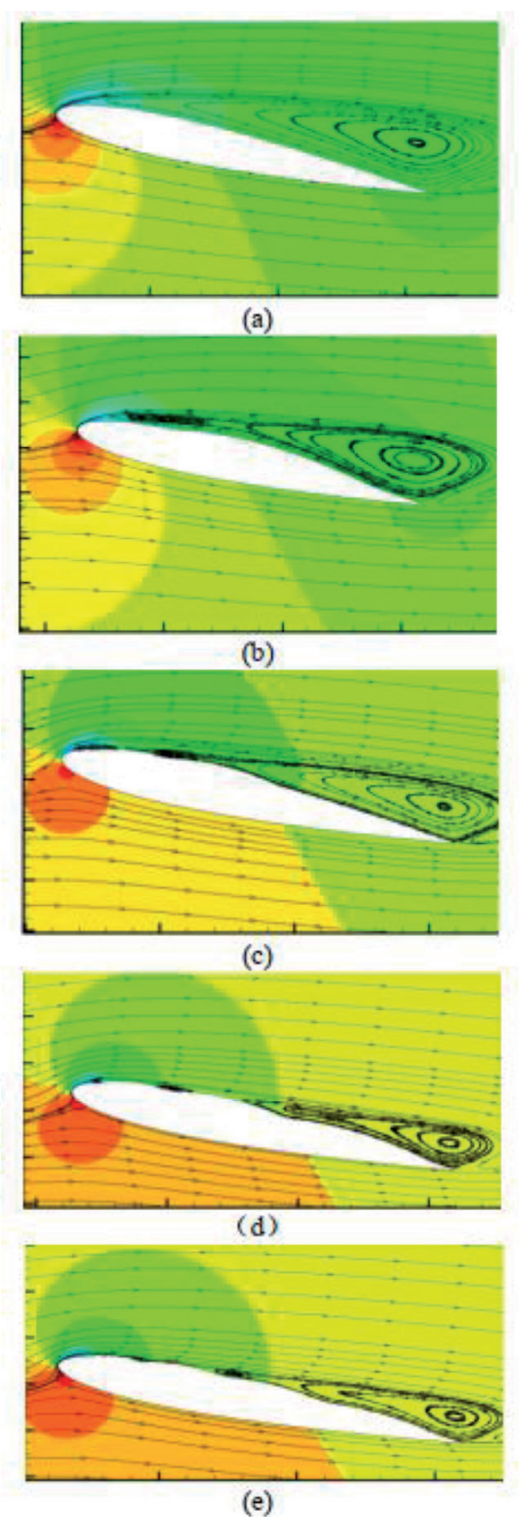


Figure 24. Streamline of rigid and flexible airfoils, $\alpha = 13^\circ$: (a) rigid; (b) one-segment; (c) two-segment; (d) three-segment; and (e) four-segment [95].

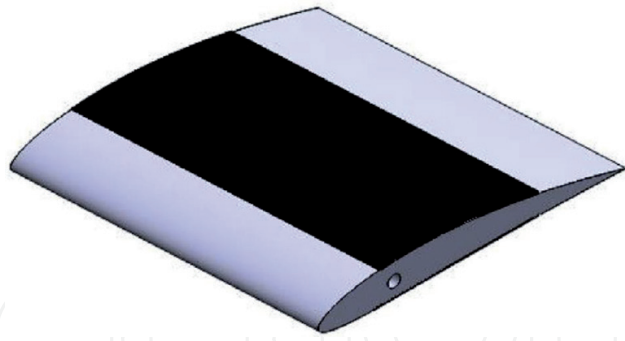


Figure 25. Configuration of the partially flexible airfoil [99].

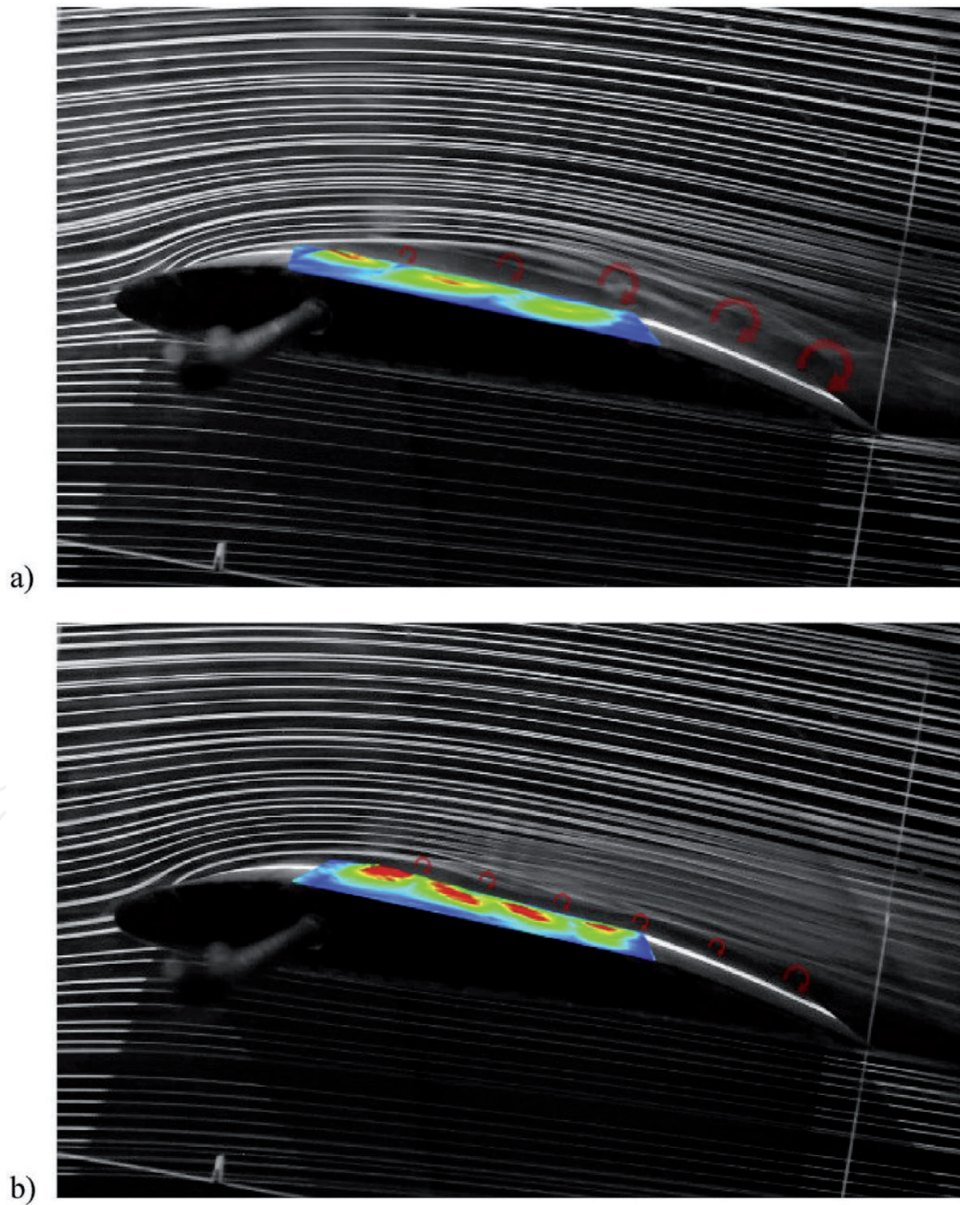


Figure 26. Integrated sketch of the flow visualization and standard deviation of the deformation at $\alpha = 8^\circ$ for (a) $Re = 2.5 \times 10^4$ and (b) $Re = 5 \times 10^4$ [99].

membrane material was used on the suction side of the airfoil. They numerically modeled four different cases on which the upper surface of the airfoil was flexible. In this numerical model, the effect of flexibility on aerodynamic performance in various regions on the airfoil was investigated for a Reynolds number of 1.35×10^5 . **Figure 24** [95] gives information about flow over the uncontrolled airfoil and the segmented flexible airfoils. It has been observed that the interaction between flow and the segmented airfoil decreases flow separations at high angles of attack. It has been found that the airfoil with three separate flexible zones shows the best aerodynamic performance and increased the lift coefficient by 39% compared to the rigid airfoil around the stall angle.

Apart from numerical study, first detailed experimental investigations on a partially flexible airfoil at low Reynolds numbers were carried out by Açıkel and Genç [99]. They modified the rigid NACA 4412 airfoil by using a membrane material that was located on the upper side of the airfoil as denoted in **Figure 25** [99]. The location of the membrane was between $x/c = 0.2$ and $x/c = 0.7$. In this study, different experimental methods such as force measurement, velocity measurement, deformation measurement, and smoke wire visualization were used to investigate flow control on partially flexible membrane airfoil.

According to the experimental results, flow control with flexibility is more effective at low angles of attack. **Figure 26** [99] demonstrates a combined sketch of the membrane standard deviation and smoke wire visualization for $\alpha = 8^\circ$. This sketch showed that the membrane vibration modes were increased with increasing Reynolds number.

4. Conclusion

A detailed review with regard to passive control methods affecting the flow especially at low Reynolds numbers was presented in this chapter. The main purpose of this study is to clarify the passive control techniques for UAVs and MAVs operating at low Reynolds numbers. Besides the explanation of those techniques, especially three passive flow methods at low Reynolds numbers have been highlighted with their results as follows:

- Using the sandpaper as a passive flow controller [8, 69] on the surface of the airfoil has caused the LSB's size to reduce enormously, resulting in aerodynamic performance recovery. Moreover, the roughness-induced transition phenomenon also mentioned in studies performed by Puckert and Rist [100] and Bucci et al. [101] has occurred with the usage of sandpaper. Therefore, a more stable flow characteristic has been obtained.
- Time-dependent attitudes of LSB obtained from results of flexible membrane wings [74] showed that bubble size first increased and then reduced at different low Reynolds numbers and angles of attack. That is, it can be understood that fluid-structure interaction positively exhibited a good effect on aerodynamic performance by varying the bubble size with time.
- Regarding the usage of the partially flexible airfoil [99], flow control in conjunction with partial flexibility is more effective especially at low angles of attack. Both flow and flexibility-induced undulation over membrane material have caused the vibration modes, helping

the bubble size to be reduced. Thus, better aerodynamic performance with the increasing of lift coefficient has been obtained.

Consequently, this detailed chapter will present a comprehensive, practical, effective road-map for the aerodynamic researchers especially interested in the flow control techniques over wind turbine blade or MAV applications operating at low Reynolds number regimes.

Nomenclature

Abbreviation

LSB	laminar separation bubble
UAV	unmanned aerial vehicle
MAV	micro air vehicle
Ma	Mach number
2D	two dimensional
3D	three dimensional
POD	proper orthogonal decomposition
DIC	digital image correlation
AR	aspect ratio
FSI	fluid-structure interaction
LE	leading edge
TE	trailing edge
VG	vortex generator
CFD	computational fluid dynamics
APG	adverse pressure gradient
AoA	angle of attack

Symbols

Re	Reynolds number
Re _c	critical Reynolds number
c	chord length of airfoil

s	span length of membrane wing
h	height of VG
b	cropped edge length of VG
L	vane length of VG
D	long gaps among vanes
d	short gaps among vanes
β	inflow angle
X	slot position
γ	slot width
ψ	angle between slot axis and chord normal
t	time
C_L	lift coefficient
C_D	drag coefficient
k	roughness height
α	angle of attack
$C_{L, \max}$	maximum lift coefficient

Subscripts

L	lift
D	drag
max	maximum
c	critical

Author details

Mustafa Serdar Genç^{1*}, Kemal Koca¹, Hacımurat Demir^{1,2} and Halil Hakan Açikel¹

*Address all correspondence to: musgenc@erciyes.edu.tr

1 Wind Engineering and Aerodynamic Research Center, Department of Energy Systems Engineering, Erciyes University, Kayseri, Turkey

2 Department of Mechanical Engineering, Aksaray University, Aksaray, Turkey

References

- [1] Arcara PC Jr, Bartlett DW, McCullers LA. Analysis for the application of hybrid laminar flow control to a long-range subsonic transport aircraft. Society of Automotive Engineers SAE 9121. 1991
- [2] Horton HP. Laminar separation in two and three-dimensional incompressible flow [PhD thesis]. University of London; 1968
- [3] Gaster M. The structure and behaviour of laminar separation bubbles. ARC Reports and Memoranda 3595. London, UK: Aeronautical Research Council (ARC); 1967
- [4] Genç MS, Karasu I, Açikel HH, Akpolat MT. Low Reynolds number flows and transition, low Reynolds number aerodynamics and transition. In: Serdar GENÇ M, editor. Rijeka, Croatia: InTech-Open Access; 2012. pp. 1-28. ISBN: 978-953-51-0492-6
- [5] Diwan SS, Chetan SJ, Ramesh ON. On the bursting criterion for laminar separation bubbles. In: IUTAM Symposium on Laminar-Turbulent Transition. Dordrecht: Springer; 2006. pp. 401-407
- [6] Boiko AV, Grek GR, Dovgal AV, Kozlov VV. The Origin of Turbulence in near-Wall Flows. Berlin, Germany: Springer Science & Business Media; 2013
- [7] Dovgal AV, Kozlov VV, Michalke A. Laminar boundary layer separation: Instability and associated phenomena. Progress in Aerospace Sciences. 1994;**30**(1):61-94
- [8] Genç MS, Koca K, Açikel HH. Investigation of pre-stall flow control on wind turbine blade airfoil using roughness element. Energy. 2019;**176**:320-334
- [9] Prandtl L. Bemerkungen über die Entstehung der Turbulenz. ZAMM-Journal of Applied Mathematics and Mechanics/Zeitschrift für Angewandte Mathematik und Mechanik. 1921;**1**(6):431-436
- [10] Tollmien W. Über die entstehung der turbulenz. In: Vorträge aus dem Gebiete der Aerodynamik und verwandter Gebiete. Berlin, Heidelberg: Springer; 1930. pp. 18-21
- [11] Schubauer GB, Skramstad HF. Laminar boundary layer oscillations and the stability of laminar flow. Journal of Aerosol Science. 1947;**14**:69-78
- [12] Mayle RE. The role of laminar-turbulent transition in gas turbine engines. Journal of Turbomachinery. 1991;**113**:509-537
- [13] Kurelek J. Transition in a laminar separation bubble and the effect of acoustic excitation [master's thesis]. University of Waterloo; 2016
- [14] Bertolotti F. Linear and nonlinear stability of boundary layers with streamwise varying properties [Ph.D. thesis]. 1991
- [15] Schlichting H, Gersten K. Boundary Layer Theory. Berlin, Heidelberg: Springer-Verlag; 2000

- [16] Langtry R, Menter F. Overview of Industrial Transition Modelling in CFX. Otterfing, Germany: ANSYS Germany GmbH, ANSYS CFX; 2006
- [17] Narasimha R, Sreenivasan KR. Relaminarization of fluid flows. *Advances in Applied Mechanics*. vol. 19. 1979. pp. 221-309
- [18] Badrya C, Govindarajan B, Chopra I. Basic understanding of unsteady airfoil aerodynamics at low Reynolds numbers. In: 2018 AIAA Aerospace Sciences Meeting. 2018. p. 2061
- [19] Pechlivanoglou G. *Passive and Active Flow Control Solutions for Wind Turbine Blades*. 2013
- [20] Seshagiri A, Cooper E, Traub LW. Effects of vortex generators on an airfoil at low Reynolds numbers. *Journal of Aircraft*. 2009;**46**(1):116-122
- [21] Aider JL, Beaudoin JF, Wesfreid JE. Drag and lift reduction of a 3D bluff-body using active vortex generators. *Experiments in Fluids*. 2010;**48**(5):771-789
- [22] Lee S, Loth E. Supersonic boundary-layer interactions with various micro-vortex generator geometries. *The Aeronautical Journal*. 2009;**113**(1149):683-697
- [23] Wang H, Zhang B, Qiu Q, Xu X. Flow control on the NREL S809 wind turbine airfoil using vortex generators. *Energy*. 2017;**118**:1210-1221
- [24] Langan K, Samuels J. Experimental investigation of maneuver performance enhancements on an advanced fighter/attack aircraft. In: 33rd Aerospace Sciences Meeting and Exhibit. 1995. p. 442
- [25] Farzaneh-Gord M, Sadi M. Improving vortex tube performance based on vortex generator design. *Energy*. 2014;**72**:492-500
- [26] Zhou G, Pang M. Experimental investigations on thermal performance of phase change material—Trombe wall system enhanced by delta winglet vortex generators. *Energy*. 2015;**93**:758-769
- [27] Taylor HD. The elimination of diffuser separation by vortex generators. Technical Report No, 4012, 3. East Hartford, CT: United Aircraft Corporation; 1947
- [28] Schubauer GB, Spangenberg WG. Forced mixing in boundary layers. *Journal of Fluid Mechanics*. 1960;**8**(1):10-32
- [29] Lin JC, Robinson SK, McGhee RJ, Valarezo WO. Separation control on high-lift airfoils via micro-vortex generators. *Journal of Aircraft*. 1994;**31**(6):1317-1323
- [30] Nickerson JR. A study of vortex generators at low Reynolds numbers. In: 24th Aerospace Sciences Meeting. 1986. p. 155
- [31] Gao L, Zhang H, Liu Y, Han S. Effects of vortex generators on a blunt trailing-edge airfoil for wind turbines. *Renewable Energy*. 2015;**76**:303-311

- [32] Bragg MB, Gregorek GM. Experimental study of airfoil performance with vortex generators. *Journal of Aircraft*. 1987;**24**(5):305-309
- [33] Baldacchino D, Ferreira C, Tavernier DD, Timmer WA, van Bussel GJW. Experimental parameter study for passive vortex generators on a 30% thick airfoil. *Wind Energy*. Vol. 21. 2018. pp. 745-765
- [34] Godard G, Stanislas M. Control of a decelerating boundary layer. Part 1: Optimization of passive vortex generators. *Aerospace Science and Technology*. 2006;**10**(3):181-191
- [35] Handley PF. Wing and similar member of aircraft. U.S. Patent No 1,427,012. 1922
- [36] Van Dam CP. The aerodynamic design of multi-element high-lift systems for transport airplanes. *Progress in Aerospace Sciences*. 2002;**38**(2):101-144
- [37] Richard PR, Wilkins SJ, Hall JW. Particle image velocimetry investigation of the coherent structures in a leading-edge slat flow. *Journal of Fluids Engineering*. 2018;**140**(4):041105
- [38] Rumsey CL, Ying SX. Prediction of high lift: Review of present CFD capability. *Progress in Aerospace Sciences*. 2002;**38**(2):145-180
- [39] Weick FE, Shortall JA. The Effect of Multiple Fixed Slots and a Trailing-Edge Flap on the Lift and Drag of a Clark y Airfoil. 1933
- [40] Weick FE, Platt RC. Wind-Tunnel Tests on Model Wing with Fowler Flap and Specially Developed Leading-Edge Slot. 1933
- [41] Krüger W. Wind-Tunnel Investigations on a Changed Mustang Profile with Nose Flap Force and Pressure-Distribution Measurements. 1947
- [42] Genç MS, Kaynak Ü, Lock GD. Flow over an aerofoil without and with a leading-edge slat at a transitional Reynolds number. *Proceedings of the Institution of Mechanical Engineers, Part G: Journal of Aerospace Engineering*. 2009;**223**(3):217-231
- [43] Fish FE, Lauder GV. Passive and active flow control by swimming fishes and mammals. *Annual Review of Fluid Mechanics*. 2006;**38**:193-224
- [44] Ibrahim IH, New TH. Tubercle modifications in marine propeller blades. In: 10th Pacific Symposium on Flow Visualization and Image Processing. Italy: Naples. p. 2015
- [45] Post ML, Decker R, Sapell AR, Hart JS. Effect of bio-inspired sinusoidal leading-edges on wings. *Aerospace Science and Technology*. 2018;**81**:128-140
- [46] Wang Z, Zhuang M. Leading-edge serrations for performance improvement on a vertical-axis wind turbine at low tip-speed-ratios. *Applied Energy*. 2017;**208**:1184-1197
- [47] Cai C, Zuo Z, Liu S, Maeda T. Effect of a single leading-edge protuberance on NACA 634-021 airfoil performance. *Journal of Fluids Engineering*. 2018;**140**(2):021108
- [48] Wei Z, New TH, Cui YD. An experimental study on flow separation control of hydrofoils with leading-edge tubercles at low Reynolds number. *Ocean Engineering*. 2015;**108**:336-349

- [49] Belamadi R, Djemili A, Ilinca A, Mdouki R. Aerodynamic performance analysis of slotted airfoils for application to wind turbine blades. *Journal of Wind Engineering and Industrial Aerodynamics*. 2016;**151**:79-99
- [50] Beyhaghi S, Amano RS. A parametric study on leading-edge slots used on wind turbine airfoils at various angles of attack. *Journal of Wind Engineering and Industrial Aerodynamics*. 2018;**175**:43-52
- [51] Shi X, Xu S, Ding L, Huang D. Passive flow control of a stalled airfoil using an oscillating micro-cylinder. *Computers & Fluids*. 2019;**178**:152-165
- [52] Luo D, Huang D, Sun X. Passive flow control of a stalled airfoil using a microcylinder. *Journal of Wind Engineering and Industrial Aerodynamics*. 2017;**170**:256-273
- [53] Wang Y, Li G, Shen S, Huang D, Zheng Z. Investigation on aerodynamic performance of horizontal axis wind turbine by setting micro-cylinder in front of the blade leading edge. *Energy*. 2018;**143**:1107-1124
- [54] Wang JJ, Li YC, Choi KS. Gurney flap-lift enhancement, mechanisms and applications. *Progress in Aerospace Sciences*. 2008;**44**(1):22-47
- [55] Liebeck RH. Design of subsonic airfoils for high lift. *Journal of Aircraft*. 1978;**15**(9):547-561
- [56] Zhu B, Huang Y, Zhang Y. Energy harvesting properties of a flapping wing with an adaptive Gurney flap. *Energy*. 2018;**152**:119-128
- [57] Shukla V, Kaviti AK. Performance evaluation of profile modifications on straight-bladed vertical axis wind turbine by energy and Spalart Allmaras models. *Energy*. 2017;**126**:766-795
- [58] Meyer R, Hage W, Bechert DW, Schatz M, Knacke T, Thiele F. Separation control by self-activated movable flaps. *AIAA Journal*. 2007;**45**(1):191-199
- [59] Rosti ME, Omidyeganeh M, Pinelli A. Passive control of the flow around unsteady aerofoils using a self-activated deployable flap. *Journal of Turbulence*. 2018;**19**(3):204-228
- [60] Arivoli D, Singh I. Self-adaptive flaps on low aspect ratio wings at low Reynolds numbers. *Aerospace Science and Technology*. 2016;**59**:78-93
- [61] Schluter JU. Lift enhancement at low Reynolds numbers using self-activated movable flaps. *Journal of Aircraft*. 2010;**47**(1):348-351
- [62] Kasper W. Aircraft wing with vortex generation. U.S. Patent No 3,831,885. 1974
- [63] Olsman WFJ, Colonius T. Numerical simulation of flow over an airfoil with a cavity. *AIAA Journal*. 2011;**49**(1):143-149
- [64] Lam GC, Leung RC. Aeroacoustics of NACA 0018 airfoil with a cavity. *AIAA Journal*. 2018;**56**(3):1-12
- [65] Li Q, Liu C. LES for supersonic ramp control flow using MVG at $M = 2.5$ and $Re_0 = 1440$. In: 48th AIAA Aerospace Sciences Meeting Including the New Horizons Forum and Aerospace Exposition. 2010. p. 592

- [66] Huebsch WW. Numerical Investigation on the Interaction between Surface Roughness and Viscous Flows. 2000
- [67] Koca K, Genç MS, Açikel HH, Çağdaş M, Bodur TM. Identification of flow phenomena over NACA 4412 wind turbine airfoil at low Reynolds numbers and role of laminar separation bubble on flow evolution. *Energy*. 2018;**144**:750-764
- [68] Genç MS, Koca K, Açikel HH, Özkan G, Kırış MS, Yıldız R. Flow characteristics over NACA4412 airfoil at low Reynolds number. In: EPJ Web of Conferences. EDP Sciences. 2016. p. 02029
- [69] Koca K, Genç MS, Açikel HH. Rüzgar Türbini Kanadı Üzerindeki Yüzey Pürüzlülüğü Etkisinin Deneysel İncelenmesi. *Çukurova Üniversitesi Mühendislik-Mimarlık Fakültesi Dergisi*. 2016;**31**:127-134
- [70] Shyy W, Berg M, Ljungqvist D. Flapping and flexible wings for biological and micro air vehicles. *Progress in Aerospace Sciences*. 1999;**35**(5):455-505
- [71] Timpe A, Zhang Z, Hubner J, Ukeiley L. Passive flow control by membrane wings for aerodynamic benefit. *Experiments in Fluids*. 2013;**54**(3):1471
- [72] Smith MJ. Simulating moth wing aerodynamics-towards the development of flapping-wing technology. *AIAA Journal*. 1996;**34**(7):1348-1355
- [73] Mueller TJ, DeLaurier JD. Aerodynamics of small vehicles. *Annual Review of Fluid Mechanics*. 2003;**35**(1):89-111
- [74] Demir H, Genç MS. An experimental investigation of laminar separation bubble formation on flexible membrane wing. *European Journal of Mechanics-B/Fluids*. 2017;**65**:326-338
- [75] Genç MS, Demir H, Açikel HH. Time dependent laminar separation bubble formation and deformation over flexible membrane wing. In: The International Symposium on Sustainable Aviation (ISSA-2016); 29 May-1 June 2016; Istanbul, Turkey
- [76] Genç MS, Açikel HH, Demir H, Özden M, Çağdaş M, Isabekov I. Effect of tip vortices on membrane vibration of flexible wings with different aspect ratios. In: EPJ Web of Conferences. EDP Sciences. 2016. p. 02028
- [77] Genç MS, Özden M, Açikel HH, Demir H, Isabekov I. Unsteady flow over flexible wings at different low Reynolds numbers. In: EPJ Web of Conferences. EDP Sciences. 2016. p. 02030
- [78] Rojratsirikul P, Genc MS, Wang Z, Gursul I. Flow-induced vibrations of low aspect ratio rectangular membrane wings. *Journal of Fluids and Structures*. 2011;**27**(8):1296-1309
- [79] Rojratsirikul P, Wang Z, Gursul I. Effect of pre-strain and excess length on unsteady fluid-structure interactions of membrane airfoils. *Journal of Fluids and Structures*. 2010;**26**(3):359-376

- [80] Genç MS. Unsteady aerodynamics and flow-induced vibrations of a low aspect ratio rectangular membrane wing with excess length. *Experimental Thermal and Fluid Science*. 2013;**44**:749-759
- [81] Greenhalgh S, Curtiss HC, Smith B. Aerodynamic properties of a two-dimensional inextensible flexible airfoil. *AIAA Journal*. 1984;**22**(7):865-870
- [82] Arbós-Torrent S, Ganapathi-subramani B, Palacios R. Leading-and trailing-edge effects on the aeromechanics of membrane aerofoils. *Journal of Fluids and Structures*. 2013; **38**:107-126
- [83] Galvao R, Israeli E, Song A, Tian X, Bishop K, Swartz S, et al. The aerodynamics of compliant membrane wings modeled on mammalian flight mechanics. In: 36th AIAA Fluid Dynamics Conference and Exhibit. 2006. p. 2866
- [84] Bleischwitz R, De Kat R, Ganapathisubramani B. Aeromechanics of membrane wings in ground-effect. In: 45th AIAA Fluid Dynamics Conference. 2015. p. 2764
- [85] Hu H, Kumar AG, Abate G, Albertani R. An experimental investigation on the aerodynamic performances of flexible membrane wings in flapping flight. *Aerospace Science and Technology*. 2010;**14**(8):575-586
- [86] Albertani R, Stanford B, Hubner JP, Ifju PG. Aerodynamic coefficients and deformation measurements on flexible micro air vehicle wings. *Experimental Mechanics*. 2007;**47**(5):625-635
- [87] Osterberg N. Experimental investigation of dynamic stall on pliant wings for micro air vehicles. In: 54th AIAA Aerospace Sciences Meeting. 2016. p. 0146
- [88] Song A, Tian X, Israeli E, Galvao R, Bishop K, Swartz S, et al. Aeromechanics of membrane wings with implications for animal flight. *AIAA Journal*. 2008;**46**(8):2096-2106
- [89] Rojratsirikul P, Wang Z, Gursul I. Unsteady aerodynamics of membrane airfoils. In: 46th AIAA Aerospace Sciences Meeting and Exhibit. 2008. p. 613
- [90] Rojratsirikul P, Wang Z, Gursul I. Unsteady fluid–structure interactions of membrane airfoils at low Reynolds numbers. *Experiments in Fluids*. 2009;**46**(5):859
- [91] Tamai M, Murphy J, Hu H. An experimental study of flexible membrane airfoils at low Reynolds numbers. In: 46th AIAA Aerospace Sciences Meeting and Exhibit. 2008. p. 580
- [92] Wrist AH, Zhang Z, Pepley D, Hubner JP. Aerodynamic comparison of flat and cambered frames for flexible MAV wings. In: 53rd AIAA Aerospace Sciences Meeting. 2015. p. 1299
- [93] Attar PJ, Morris BJ, Romberg WA, Johnston JW, Parthasarathy RN. Experimental characterization of aerodynamic behavior of membrane wings in low-Reynolds-number flow. *AIAA Journal*. 2012;**50**(7):1525-1537

- [94] Viieru D, Tang J, Lian Y, Liu H, Shyy W. Flapping and flexible wing aerodynamics of low Reynolds number flight vehicles. In: 44th AIAA Aerospace Sciences Meeting and Exhibit. 2006. p. 503
- [95] Hefeng D, Chenxi W, Shaobin L, Zhen SX. Numerical research on segmented flexible airfoils considering fluid-structure interaction. *Procedia Engineering*. 2015;**99**:57-66
- [96] Lian Y, Shyy W. Laminar-turbulent transition of a low Reynolds number rigid or flexible airfoil. *AIAA Journal*. 2007;**45**(7):1501-1513
- [97] Gordnier RE, Attar PJ. Impact of flexibility on the aerodynamics of an aspect ratio two membrane wing. In: ASME 2012 Fluids Engineering Division Summer Meeting collocated with the ASME 2012 Heat Transfer Summer Conference and the ASME 2012 10th International Conference on Nanochannels, Microchannels, and Minichannels. American Society of Mechanical Engineers; 2012. pp. 1481-1496
- [98] Demir H. Investigation of Unsteady Aerodynamics of Flexible Wings at Low Reynolds Numbers, PhD. Thesis. Turkey: Erciyes University; 2018
- [99] Açıkel HH, Genç MS. Control of laminar separation bubble over wind turbine airfoil using partial flexibility on suction surface. *Energy*. 2018;**165**:176-190
- [100] Puckert DK, Rist U. Experiments on critical Reynolds number and global instability in roughness-induced laminar-turbulent transition. *Journal of Fluid Mechanics*. 2018;**844**:878-904
- [101] Bucci MA, Puckert DK, Andriano C, Loiseau JC, Cherubini S, Robinet JC, et al. Roughness-induced transition by quasi-resonance of a varicose global mode. *Journal of Fluid Mechanics*. 2018;**836**:167-191